JOURNAL OF NEUROTRAUMA 35:1800–1818 (August 1, 2018)

DOI: 10.1089/neu.2017.5605

Effects of Mitochondrial Transplantation on Bioenergetics, Cellular Incorporation, and Functional Recovery after Spinal Cord Injury

Jenna L. Gollihue,[1,2] Samir P. Patel,[1,2] Khalid C. Eldahan,[1,2] David H. Cox,[2] Renee R. Donahue,[1] Bradley K. Taylor,[1,2] Patrick G. Sullivan,[2,3] and Alexander G. Rabchevsky[1,2]

Abstract

Our previous studies reported that pharmacological maintenance of mitochondrial bioenergetics after experimental spinal cord injury (SCI) provided functional neuroprotection. Recent evidence indicates that endogenous mitochondrial transfer is neuroprotective as well, and, therefore, we extended these studies with a novel approach to transplanting exogenous mitochondria into the injured rat spinal cord. Using a rat model of L1/L2 contusion SCI, we herein report that transplantation of exogenous mitochondria derived from either cell culture or syngeneic leg muscle maintained acute bioenergetics of the injured spinal cord in a concentration-dependent manner. Moreover, transplanting transgenically labeled turbo green fluorescent (tGFP) PC12-derived mitochondria allowed for visualization of their incorporation in both a time-dependent and cell-specific manner at 24 h, 48 h, and 7 days post-injection. tGFP mitochondria co-localized with multiple resident cell types, although they were absent in neurons. Despite their contribution to the maintenance of normal bioenergetics, mitochondrial transplantation did not yield long-term functional neuroprotection as assessed by overall tissue sparing or recovery of motor and sensory functions. These experiments are the first to investigate mitochondrial transplantation as a therapeutic approach to treating spinal cord injury. Our initial bioenergetic results are encouraging, and although they did not translate into improved long-term outcome measures, caveats and technical hurdles are discussed that can be addressed in future studies to potentially increase long-term efficacy of transplantation strategies.

Keywords: Basso, Beattie, Bresnahan locomotor rating scale; mitochondrial respiration; transgenic labeling; Von Frey hair test

Introduction

Contusion spinal cord injury (SCI) can result in lifelong debilitation and has a profound impact on the day to day activities of individuals living with SCI. In the event of an injury, the primary injury site comprises necrotic tissue that triggers secondary injury cascades, including glutamate excitotoxicity, decreased adenosine triphosphate (ATP) production, increased lipid and protein oxidation, and resulting apoptosis and necrosis (see the studies by Dumont and coworkers[1] and Rowland and coworkers[2] for a comprehensive review of pathophysiology following SCI). Mitochondrial dysfunction is intimately related to detrimental secondary pathophysiology resulting from SCI, and is pivotal to injury progression and disease in other models including traumatic brain injury (TBI), cardiac ischemia, stroke, Parkinson's disease (PD), and Alzheimer's disease.[3–13] As such, mitochondrial medicine is a developing field of therapeutics aimed at improving mitochondrial health and function for a variety of physiological disease and injury states. Using different methods to target mitochondria dysfunction, multiple groups have reported that this yields neuroprotection, tissue sparing, and functional recovery. For example, in models of nephrotoxicity, TBI, SCI, PD, neurodegeneration, and oxidative stress, antioxidants decrease the reactive oxygen species (ROS) and reactive nitrogen species (RNS) damage caused by dysfunctional mitochondria.[14–24] Mild uncoupling of the electron transport system (ETS) increases ATP production following neurological insult *in vitro* and quinolinic acid neurological injury *in vivo*, and is therapeutic for the recovery from mitochondrial dysfunction after SCI.[25–30] Mitochondrial substrate precursors such as acetyl L-carnitine (ALC) and *N*-acetylcysteine amide (NACA) improve mitochondrial function and behavioral recovery after TBI and SCI, as well as in PD and age-related cognitive functional decline.[24,31–37] In summary, interventions that alleviate mitochondrial dysfunction exert a broad spectrum of therapeutic benefits across a wide range of disorders.

Mitochondrial transplantation is emerging as a potential therapeutic to maintain mitochondrial function after injury, consequently improving long-term functional outcome.[38] The mechanisms by which transplanted mitochondria exert beneficial effects may

Departments of [1]Physiology and [3]Neuroscience, and [2]Spinal Cord & Brain Injury Research Center, University of Kentucky, Lexington, Kentucky.

include: increases in ATP production and calcium buffering capacity, decreases in overall ROS production, and generation of a new pool of mitochondrial DNA (mtDNA) (for a review see the study by Gollihue and Rabchevsky[39]). Although this therapy is relatively new, mitochondrial transplantation is effective in promoting recovery after ischemic injury to cardiac tissue.[7,40–42] More recently, astrocytes were found to inherently donate their mitochondria to nearby neurons after stroke injury *in vivo*, and astrocytes can be further induced to release mitochondria after injury, both of which can contribute to functional neuroprotection.[43] Indeed, pharmacological blockade of astrocyte donation of mitochondria inhibited mitochondrial transfer and resulted in neuronal cell death, demonstrating the importance of mitochondrial transfer into damaged cells for cell survival. Further, intravenous injections of isolated fluorescently labeled mitochondria in a mouse model of PD resulted in a decrease in ROS along with increases in ATP production, complex I activity, and behavioral scores compared with vehicle-injected animals.[44] In a rat model of PD, injections of Pep-1 conjugated isolated mitochondria into the medial forebrain bundle increased locomotor scores and dopaminergic neuronal sparing.[45] Additional premise for the current studies is based on our recent report that exogenous transgenically labeled mitochondria can be incorporated into cells both *in vitro* and in rat spinal cords at 24 and 48 h post-transplantation.[46]

Herein, we investigated the therapeutic effects of mitochondrial transplantation immediately after SCI. We hypothesized that supplementation of the injured spinal cord with a pool of healthy, well-coupled mitochondria would provide a new source of increased energy production, decreased oxidation, and dampened effects of glutamate excitotoxicity, resulting in maintenance of tissue bioenergetics. We further posited that exogenous mitochondria would incorporate into a variety of cell types and that the beneficial effects in the short term would result in long-term benefits such as tissue sparing and improvements in hindlimb functional recovery.

Methods

Transgenic labeling of PC12 cells

PC12 cells were transgenically labeled with a mitochondria-targeting tGFP, as previously described.[46] Briefly, PC-12Adh cells were transfected with a plasmid vector containing tGFP and a mitochondrial targeting sequence for the cytochrome c oxidase complex subunit VIII. Following transfection, cells were kept under constant selection using media containing 3 μg/mL puromycin in complete media (F-12K Medium (ATCC cat # 30-2004 Manassas, VA) with 2.5% fetal bovine serum (Atlanta Biologicals # S1111OH, Atlanta, GA), 15% horse serum (Gibco # 26050-070), and 1.1% penicillin streptomycin (Corning # 30-002-CI, Tewksbury, MA).

Mitochondrial isolation from cell culture

Purified mitochondria were isolated from transfected tGFP-PC12 cells as previously described.[46] Briefly, when cells were 95% confluent they were removed manually from culture plates using a cell scraper. Mitochondria were isolated using multiple centrifugation and resuspension steps to yield Ficoll purified mitochondria. Importantly, after Ficoll purification, a thin nonmitochondrial layer was gently aspirated off the final pellet, ensuring that the sample was purified without contamination.

Mitochondrial isolation from soleus muscle

Immediately after naïve Sprague–Dawley rats ($n = 10$) were asphyxiated with CO_2 and decapitated, their soleus muscle was dissected. Each animal was placed on its stomach, with the hindlimb stretched backwards; 70% EtOH was sprayed on the hindlimb, and scissors were used to blunt dissect the skin away from the underlying calf muscle. The skin was then cut away from the muscle on the lateral sides, followed by cutting the Achilles' tendon. The muscle was pulled up and away from the leg, exposing the underlying soleus muscle. The tendons were cut at both insertion sites, and the soleus muscle was removed and placed in 2 mL of isolation buffer (215 mM mannitol, 75 mM sucrose, 0.1% bovine serum albumin [BSA], 20 mM HEPES, and pH adjusted to 7.2 with KOH) containing 1 mM EGTA and 0.025% trypsin. The muscle was chopped into smaller pieces using scissors to increase the surface area exposed to the isolation buffer and trypsin. The sample was then mechanically homogenized, with care not to introduce air bubbles. A protease inhibitor was added to halt trypsin activity, followed by centrifugation at 1500 rcf, 4°C, 5 min. The supernatant was removed and centrifuged at 13,000 rcf for 10 min at 4°C, after which the pellet was resuspended in isolation buffer and purified using Ficoll gradient (7.5%/10%) centrifugation at 32,000 rpm for 30 min, 4°C. The pellet was removed and resuspended in 0.6 mL isolation buffer without EGTA, and centrifuged at 10,000 rcf for 10 min, 4°C.The resulting pellet contain purified mitochondria that was resuspended in isolation buffer without EGTA for Pierce BCA (Thermo Fisher, cat #23225) protein assays and microinjection into spinal cords.

SCI and microinjection procedures

Adult (12 weeks old, 225–250 g) female naïve Sprague–Dawley rats (Harlan) underwent intraperitoneal injections of anesthesia (80 mg/kg ketamine and 10 mg/kg xylazine, Butler Animal Health Supply) followed by Lacri-Lube ophthalmic ointment (Medi-Vet) applied to both eyes before surgery to prevent drying. The surgical site along the dorsal spine was shaved with an electric hair trimmer and cleaned with both 70% ethanol and betadine solutions. Animals then received a T12 laminectomy to expose the L1/L2 spinal level.[37] Sham animals received a laminectomy only, whereas injured animals received a severe 250 kDyn contusion injury using a force-controlled Infinite Horizon impactor computerized injury device (Precision Systems and Instrumentation, LLC, Lexington KY).[47] Those animals that underwent SCI were split into three cohorts receiving either (1) vehicle injection, (2) cell-derived tGFP mitochondria, or (3) leg muscle-derived mitochondria; uninjured animals did not receive injections (see Table 1).

Injections were made within 30 min after injury into the mediolateral gray matter at four circumferential sites of the injured cord separated by 2mM in the rostral caudal direction (see Fig. 1) using a glass micropipette needle (World Precision Instruments, Sarasota, FL cat no. 4878) pulled and beveled to a 20–30 μm inner diameter pore opening. Each injection consisted of 750 nL of either vehicle (isolation buffer with 5 mM pyruvate, 2.5 mM malate, and 10 mM succinate) or mitochondria suspended in vehicle (for a total of 50, 100 or 150 μg); hence a total of 3 μL volume was injected per spinal cord. Muscle incisions were closed using silk sutures 3-0 Vicryl (Ethicon, Inc., Somerville, NJ), and skin incisions were closed using wound clips (Stoelting Co., Wood Dale, IL), followed by application of hydrogen peroxide and betadine. Immediately following surgery, animals were single housed in a clean cage on top of a towel on a 37°C heating pad, and monitored until recovery from anesthesia. Yohimbine (1–2 mg/kg subcutaneously [s.c.], Lloyd Laboratories) was used to counteract the effects of xylazine. Buprenorphine HCl (0.02–0.05 mg/kg s.c, Butler Animal Health Supply) was administered s.c. immediately after surgery to alleviate pain, and then every 8 h for 3 days following the operation. The antibiotic cefazolin (33.3 mg/kg, s.c, Butler Animal Health Supply) was given twice daily for 5 days postoperatively to minimize incidence of infection.

The animals were housed individually until wound clip removal, and cages were lined with absorbent pads without bedding for the

Table 1. Separation of Animal Cohorts by Outcome Measures at Different Time Points

Outcome measure	*Group*	*Dosage of mitochondria (μg)*	*Terminal time point*	n
Acute bioenergetics, oxygen consumption rate	Sham	N/A	24 h	11
	Vehicle	N/A	24 h	11
	tGFP mitochondria	50	24 h	6
		100	24 h	7
		150	24 h	6
	Muscle mitochondria	50	24 h	5
		100	24 h	6
		150	24 h	6
Immunohistochemistry-tGFP spread cell-type colocalization	Vehicle	N/A	24 h	1
			48 h	1
			7 days	1
	tGFP mitocondria	100	24 h	4
			48 h	4
			7 days	4
Long-term studies: behavior, tissue sparing, neuronal cell counts	Vehicle	N/A	6 weeks	10
	tGFP mitochondria	100	6 weeks	11
	Muscle mitochondria	100	6 weeks	8

It should be noted that in addition to these rats, 10 naïve rats were used as donors for leg muscle-derived mitochondria, and 7 rats from long-term studies were excluded for various reasons (see Results, third subsection).

duration of buprenorphine use, as pica is often observed in treated rats. After discontinuation of buprenorphine, pine bedding was used. Additional parenteral fluids (10 mL lactated Ringer's solution, Baxter Healthcare Corporation, Deerfield, IL) were provided as needed for 24–72 h post-surgery to compensate for dehydration brought on by anesthesia. Bladder expression was performed two times per day, until adequate spontaneous voiding returned to avoid urinary tract infections. Skin wound clips were removed 10–14 days post-injury with the animals under isoflurane anesthesia. Animals survived either (1) 24 h for mitochondrial respiration analyses ($n=58$); (2) 24 h, 48 h, or 7 days for histological analyses ($n=15$); or (3) 6 weeks for long-term behavioral and histological analyses ($n=36$) (see Table 1).

Behavioral analyses

The Basso, Beattie, Bresnahan (BBB) locomotor rating scale was used to analyze the hindlimb functional recovery of animals after contusion SCI. Assessments were performed according to published protocol.[48] Animals underwent contusion injury, followed by BBB assessment at 2, 7, 14, 21, 28, 35, and 42 days post-injury. Testing was performed at the same time in the same room on each testing day to reduce variation. The scores for the right and left leg were averaged for each time point. Mechanical tactile sensitivity was measured with von Frey filaments (Stoelting, Inc, Wood Dale, IL) as previously described[49] and modified.[50,51] The hindpaw was stimulated with an incremental series of eight monofilaments of increasing logarithmic stiffness. A modified up-down method was used to determine the 50% withdrawal threshold. An intermediate force von Frey filament (#4.31, 2.0*g* force) was first applied to the glabrous skin until the filament was slightly bent. In case of a positive response (withdraw of the paw within 2 sec), the next filament of lesser force was applied. In the case of a negative response, the next filament greater force was applied. The thresholds for both hindpaws were averaged and reported.

Mitochondrial isolation from spinal cords

For bioenergetics assays, animals were CO_2 asphyxiated and decapitated 24 h after injury and injections. A 1 cm segment of spinal cord surrounding the injury site and including all of the injection sites was quickly dissected, and total mitochondria were isolated as described previously.[13,17,37] Briefly, the spinal cord was placed in a homogenization tube with 2 mL isolation buffer containing EGTA ([215 mM mannitol, 75 mM sucrose, 0.1% BSA, 20 mM HEPES, and pH adjusted to 7.2 with KOH] containing 1 mM EGTA), and physically homogenized with six quick rotations of the pestle, without introducing air bubbles into the solution. The sample was poured into a 2 mL Eppendorf tube and centrifuged at 1400 rcf for 3 min, 4°C. The supernatants containing mitochondria were then poured into a separate Eppendorf tube, and this tube was filled up to 2 mL with isolation buffer containing EGTA. To increase yield, the pellet from the previous spin was resuspended in 500 μL isolation buffer containing EGTA and again centrifuged at 1400 rcf for 3 min at 4°C. The supernatants containing mitochondria from this spin was again poured into separate tubes and filled to 2mL with isolation buffer containing EGTA. The supernatant tubes were then centrifuged at 13,000 rcf for 10 min at 4°C. The resulting supernatant was discarded, and 350 μL isolation buffer containing EGTA was used to resuspend each pellet containing mitochondria. The samples underwent nitrogen bombing at 1200 psi for 10 min at 4°C before being placed on top of a Ficoll gradient (7.5%/10%) and centrifuged at 32,000 rpm for 30 min at 4°C. The supernatant was removed, leaving a purified mitochondrial pellet. The pellet was resuspended in 450 μL isolation buffer without EGTA and centrifuged 10,000 rcf for 10 min at 4°C to remove any remaining EGTA from the sample. The supernatant was removed, and the pellet was resuspended in isolation buffer without EGTA to a concentration of ~ 15 μg/μL. Pierce BCA protein assay was performed to determine the protein content of the sample.

Assaying respiration of isolated mitochondria

Mitochondria were assayed for oxygen consumption rate (OCR) immediately after isolation using the Seahorse Bioscience XF^e Flux Analyzer at 37°C, as described previously.[17,52] Mitochondrial respiration was assessed using a respiration buffer consisting of: 215 mM mannitol, 75 mM sucrose, 2 mM $MgCl_2$, 2.5 mM inorganic phosphates, 0.1% BSA, and 20 mM HEPES, pH 7.2. After isolation, purified mitochondria were added to the respiration buffer in the cell plate, and the cell plate was centrifuged at 2000 rpm for 4 min at 4°C to concentrate and adhere mitochondria to the bottom of each well. Then, 5 mM pyruvate/2.5 mM malate/1 mM

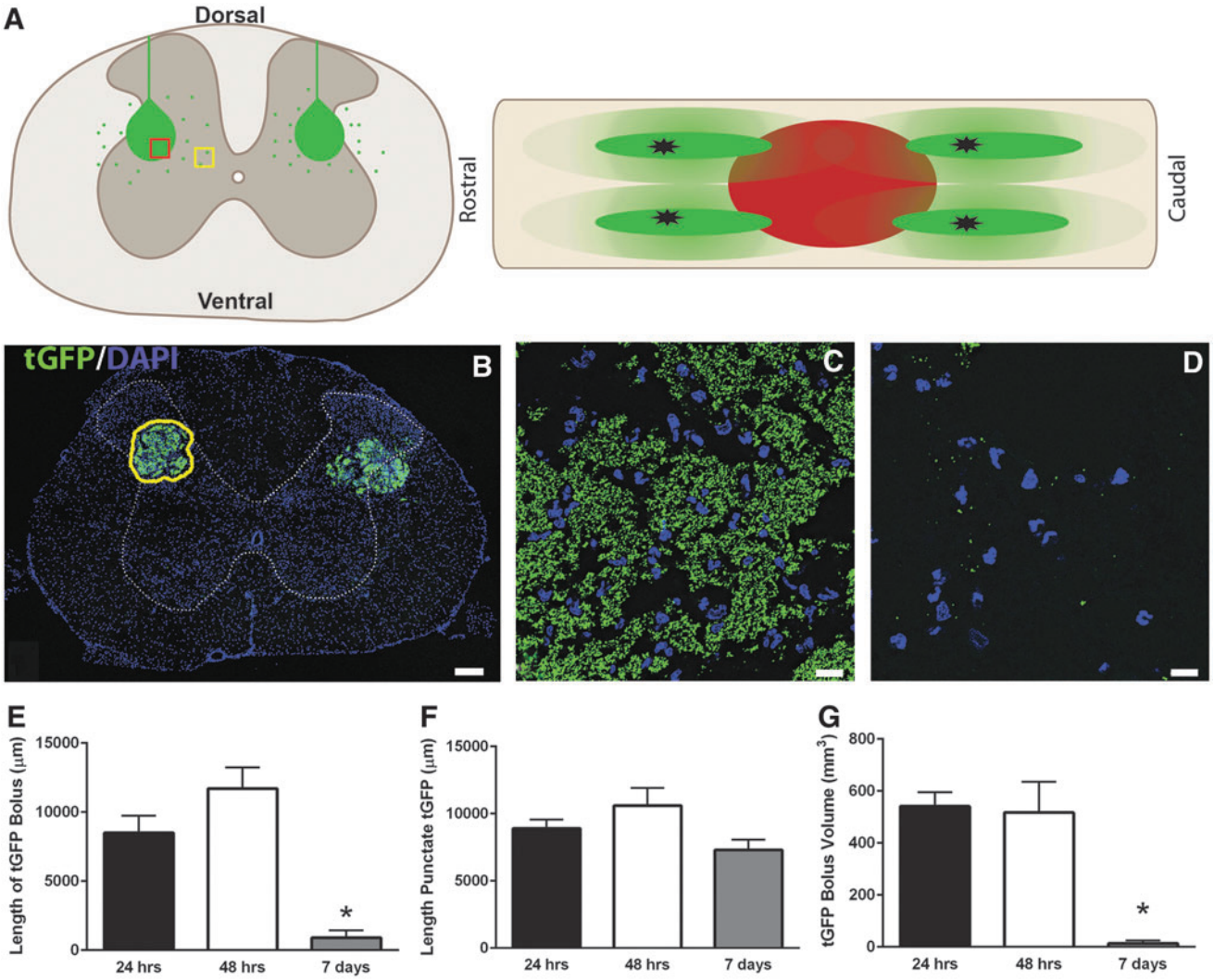

FIG. 1. Quantification of transplanted tGFP mitochondria distribution. **(A)** Schematics depict location of mitochondrial injections into the spinal cord. Cross-section showing a portion of the injection bolus is boxed in red, and representation of the punctate area analyzed is boxed in yellow. Longitudinal horizontal section shows four pericontusion injection sites (black stars) with injection boluses as solid green ellipsoids. Punctate tGFP labeling is represented by the more shaded green halos. **(B)** Representative image of bilateral tGFP injections. For volumetric measurements, the discrete bolus was circled (yellow) to give an area for each section that was used to calculate the subvolume of each section measured. **(C)** High magnification image of tGFP located within the bolus of **(B)** as delineated in the red box in **(A)**. **(D)** Representative high magnification image of punctate tGFP-labeled mitochondria in **(B)** that were not part of the discreet bolus, as delineated in yellow box in **(A)**. **(E)** Rostral-caudal length of tGFP bolus was significantly decreased at 7 days compared with 24 h and 48 h groups. **(F)** Length in the rostral-caudal direction in which any visible evidence of punctate mitochondria was apparent. **(G)** tGFP injection bolus volumes significantly decreased at 7 days post-injection. Scale bars: **B** = 200 μm, **C** and **D** = 10 μm. Bars are means ± SEM. *$p < 0.05$ versus 24 and 48 h. (One way ANOVA, Tukey's multiple comparisons) $n = 4$/group. Color image is available online at www.liebertpub.com/neu

adenosine diphosphate (ADP), 1 μg/μL oligomycin, 3 μM FCCP, and 100 nM rotenone/10 mM succinate were sequentially added to each well. Oxygen levels were measured after each substrate/inhibitor addition to calculate each state of mitochondrial respiration according to published protocols.[52] Briefly, state III respiration is a measure of oxidative phosphorylation that takes place in the presence of pyruvate, malate, and ADP. State IV respiration occurs upon oligomycin addition to inhibit the ATP synthase complex, thus uncoupling the electron transport chain from the ATP synthase complex. State V.1 is mitochondrial respiration after addition of FCCP (protonophore), which collapses the inner membrane potential, and State V.2 respiration occurs after inhibition of complex 1 and addition of succinate to provide electrons through complex 2 of the electron transport chain.

Spinal cord processing for histological analyses

Rats survived to their terminal time point after injection (24 h, 48 h, 7 days, or 6 weeks). They were overdosed with 0.2 mL Fatal-Plus containing sodium pentobarbital (Vortech Pharma Ltd., Dearborn, MI) followed by transcardial perfusion with 150 mL of 0.1M phosphate buffered saline (PBS), then with 250 mL 4% paraformaldehyde (PFA) in PBS. A 3 cm segment of spinal cord centered on the L1/L2 injury site was dissected, and post-fixed up to 4 h with 4% PFA followed by washing overnight in 2M phosphate buffer. The cords were then cryoprotected in 20% sucrose/PBS at 4°C until the cords sank in the solution, then embedded in gum tragacanth (Sigma) blocks and serially cryosectioned coronally at 20 μm.[53] For the 24 h, 48 h, and 7 day cohorts, every other section

was mounted on a 10 slide series so that adjacent spinal cord sections on any given slide were spaced equally 400 μM apart. For the 6 week studies, every fifth section was mounted onto a 10 slide series with adjacent sections on a slide separated by 1000 μm.

Immunohistochemistry and fluorescent imaging

Slide-mounted spinal cord sections were washed 3 times for 5 min each in 0.1M PBS, followed by incubation in blocking buffer (0.1M PBS, 1% bovine serum albumin, 0.1% Triton-X 100, and 5% normal goat serum) for 1 h. Sections were then incubated overnight at 4°C in a primary antibody diluted to proper concentration in a blocking buffer. The next day, after being washed again, the sections were incubated with secondary antibodies overnight at 4°C before another wash, followed by 3 h incubation at room temperature in streptavidin-conjugated fluorochromes diluted to desired concentrations in 0.1M PBS. After final washes, they were coverslipped with Vectashield (Vector Labs, cat #H-1000) containing 0.5 m Hoechst dye to label nuclei (Thermo Fisher, cat# 62249). Antibodies used for epifluorescent imaging and co-localization studies included rabbit anti-tGFP (0.13μg/mL, Evrogen # Ab513), mouse anti-RECA1 (5μg/mL, abcam # ab9774), mouse anti-GFAP (2μg/mL, abcam # ab10062), mouse anti-CC1 (0.5μg/mL, Cal Biochem #OP80), mouse anti-NeuN (5μg/mL, Millipore # MAB377), mouse anti-CD11b/c (OX42, 5μg/mL, abcam # ab78457), phosphor-PDGF Receptor β (5uL/mL Cell Signaling mAb #3166), goat anti-rabbit 488 (4μg/mL, Invitrogen # A11008), goat anti-mouse Biotin (7.5μg/mL, Vector # BA-9200), and Streptavidin Texas red (3.3μg/mL, Vector # SA-5006). Z-stack images were obtained using Nikon Eclipse Ti Confocal microscope and processed with NIS Elements ND2 software (Nikon Instruments).

Quantification of tGFP mitochondria volume and spread

A set of tissue section mounted slides for each time point was used to calculate the tGFP mitochondria volume and spread over time after injection. Anti-tGFP antibody was used to label injected mitochondria, as described. Each spinal tissue section was then analyzed using the Nikon confocal microscope for the presence of distinct tGFP labeling. When a discrete tGFP injection bolus was present, Nikon NIS Elements ND2 software was used to measure the area of the bolus. Each of the four injection epicenters per spinal cord was identified by finding the largest area of discrete bolus. Every section, both rostral and caudal, of the injection epicenter that contained a discrete tGFP bolus, was measured. After defining the boundaries of the injection bolus, the section thickness and periodicity of the sectioning paradigm were used to calculate the total injection bolus volume of all four injections in each cord. The rostral-caudal lengths throughout the spinal cords where punctate tGFP labeling was evident were also calculated, regardless of apparent discrete injection boluses.

Quantification of brain macrophage response

For the 24 h, 48 h, and 7 day animal cohorts, macrophage densities at each injection epicenter were analyzed. Once the injection site was identified, based on tGFP and OX-42 immunolabeling, then a score of 0–3 was assigned for each injection epicenter, where 0 indicates normal density in macrophages (as in naïve tissues), a score of 1 indicates activation (change in morphology to an activated state with processes withdrawn), a score of 2 indicates activated brain macrophage densities in the confines of the injection site, and a score of 3 indicates brain macrophage densities that expand beyond the original injection bolus boundaries.

Time course of cell-type co-localization

Cell-type co-localization of tGFP mitochondria was quantified for different cell types in the 24 and 48 h and 7 day cohorts. Separate sets of slides were labeled for either microglia, endothelial cells, oligodendrocytes, astrocytes, pericytes, or neurons, and co-labeled with antibodies against tGFP. Eight sections total per spinal cord were assessed using the left side injections of each spinal cord including the injection epicenters, one section (400 μm) from the injection epicenter toward the injury site, one section (400 μm) from the injection epicenter away from the injury site, and the first section away from the injection epicenter that no longer contained a visible bolus (see Fig. 2A for counting schematic). The region of interest (ROI) counted for each section was the left dorsal quadrant of the spinal cord, drawing a vertical line from the central canal to the dorsal surface, and a horizontal line from the central canal to the lateral surface (see Fig. 2B for depiction of ROI). Slides were visualized under an Olympus BX51 microscope at 100x magnification (10x eye piece) using a fluorescein isothiocyanate (FITC)/tetramethylrhodamine isothiocyanate (TRITC) combination filter to simultaneously visualize the green and red fluorescent wavelengths. Co-localization was defined in two different ways. The first criterion of positive incorporation was when the tGFP labeling was evident within the confines of the labeled cell membrane, indicating that the tGFP mitochondria were within the boundaries of the cell membrane. The second criterion of positive incorporation was when the tGFP labeling was present and overlapped with the cell-specific marker within the cytoplasm and/or on cell surface. If either of these criteria were met, then this was considered a positive instance of co-localization. Sections were examined using the 4',6-diamidino-2-phenylindole (DAPI) filter to ensure that the nucleus was within the focal plane. Counts were performed within the ROI in a total of eight spinal cord sections of each animal for (1) each time a specific cell type was co-localized with tGFP and (2) total cell counts for the specific cell type. Quantification of

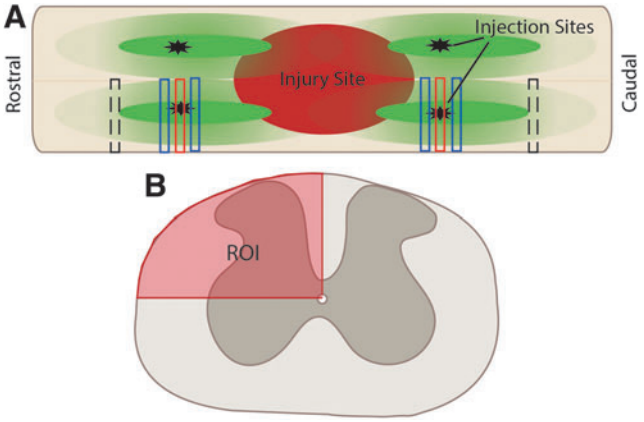

FIG. 2. Counting schematic for cell-type co-localization with tGFP mitochondria. **(A)** Eight sections were analyzed on the left side of each injected spinal cord encompassing the contusion site, including both injection epicenters (red boxes), sections 400 μm rostral and 400 μm caudal to the injection epicenters (blue boxes), and the first section distal to the injection epicenter beyond the bolus where only punctate tGFP mitochondria were present (dashed black boxes). Injection epicenters are denoted by black stars, injection boluses are depicted as solid green ovals, and punctate tGFP stippling is represented by faded light green ovals. Note that the caudal injection sites are closer to the injury because of the anatomical constraints of T12 laminectomy to effectively injure the L1/L2 spinal level. **(B)** For each section analyzed, the region of interest (ROI) for cell counts was defined by drawing a horizontal line from the central canal to the lateral side and a vertical line from the central canal to the dorsal surface (red). Both the total number of labeled specific cell types and number of instances of tGFP co-localization with a specific cell type were counted within the ROI. Color image is available online at www.liebertpub.com/neu

co-localization was reported as a percentage of tGFP-positive cells of a specific cell type divided by the total number of that specific cell type within the ROI.

Quantification of tissue sparing

Tissue sections were stained with eriochrome cyanine-cresyl violet (ECCV) to differentiate white matter and gray matter as previously described.[53,54] Mounted sections were imaged using a Nikon microscope (Nikon Corporation, Tokyo, Japan), and Scion Imaging analysis software (Scion Corporation, Frederick, MD) was used to delineate injured from spared tissue in each section. ROIs were manually drawn around the entire cord, spared gray matter, and injured tissue, which allowed extrapolation of the spared white matter area. Eleven sections equally spaced by 1000 μm (6 weeks cohort) or by 800 μm (24 and 48 h cohorts) and centered on the injury epicenter were analyzed to calculate the volume of damaged versus spared tissues using the Cavalieri method.[54,55]

Stereology

Analysis was performed to determine the number of neurons in the medial portion of lamina VII and lamina X of the L1/L2 spinal cord in the 6 week injured cohorts. Stereological counts of neurons were performed as we have previously published.[37] An Olympus BX51 microscope was used to image sections with the Bioquant image analysis program (Nova Prime, V6.70.10, Bioquant Image Analysis Corp., Nashville, TN). Briefly, an ROI was drawn over lamina VII and X, containing putative central pattern generator (CPG) interneurons. A counting grid was placed over this region, with each counting frame measuring 125 μm x 125 μm. Disectors were set to 50 μm x 50 μm, and section thickness was set at 10μm, with a 2 μm guard zone on both the top and bottom of the tissue to keep cells across sections from being double counted. Bioquant software randomly placed dissectors within the ROI, with an average of 13 disectors counted per section. NeuN-positive cells were then counted under 40x magnification (10x eyepiece). The criteria for neuron cell bodies to be counted required that they be contained within the dissector square and the nucleus be in focus within the set 10 μm counting thickness, as verified by Hoechst staining.[56]

Statistical analyses

Changes in each OCR state and respiratory control ratio (RCR) for acute bioenergetic studies, complex I functional assays, injected tGFP bolus volume and rostral-caudal length, cell-type incorporation, number of co-localization instances, and co-localization percentages within each time point were analyzed using a one way ANOVA, with Tukey's multiple comparisons post-hoc test. Macrophage density analyses were performed using a Mann–Whitney U test for each time point analyzed. Rostral-caudal co-localization studies, von Frey test, BBB scoring, and neuronal stereology counts were analyzed using a repeated measures two way ANOVA with Tukey's multiple comparisons when warranted. All analyses were performed using Graphpad Prism 6 (Graphpad Software, Inc., La Jolla, CA). Significance was set to $p < 0.05$.

Results

Transplantation Maintains Acute Mitochondrial Bioenergetics

We transplanted mitochondria into the injured spinal cord in a dose-dependent manner. Vehicle or transgenically labeled tGFP-mitochondria were microinjected into the injured spinal cord at 50, 100, or 150 μg, and 24 h later the spinal cords were dissected and assessed for mitochondrial bioenergetics from spinal cord containing both endogenous mitochondria and exogenous transplanted mitochondria. The respiration measurements in Figures 3 and 4 represent combined assessments of both host mitochondria and exogenous transplanted mitochondria, the latter of which may be either extracellular or incorporated into cells. When assayed for mitochondrial bioenergetics in terms of OCR, there were significant differences in state III (F [4, 27] = 6.269, $p = 0.0011$) and state V.1 (F [4, 27] = 11.80, $p = < 0.0001$) respiration rates among groups. Post-hoc analyses revealed that, compared with significantly impaired rates in the vehicle-injected group, the 100 μg tGFP-injected group significantly maintained state III (89% of sham) and state V.I (73% of sham) OCR (Fig. 3). There were no significant differences in RCR

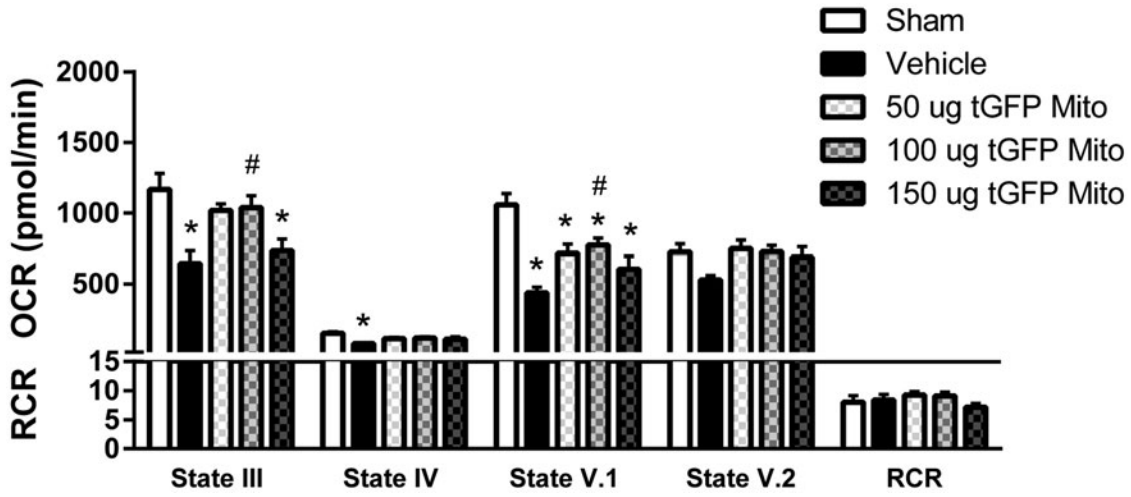

FIG. 3. tGFP mitochondrial (Mito) transplantation maintains respiration rates. SCI caused significant decreases in mitochondrial respiration at states III, IV, and V.1, which were spared partially following mitochondrial transplantation. State III and V.1 oxygen consumption rates (OCR) were maintained near sham levels after 100 μg tGFP mitochondrial transplantation. Bars are means ± SEM. *$p < 0.05$ versus sham; #$p < 0.05$ versus vehicle. (One way ANOVA for each state, Tukey's multiple comparison) $n = 6$–7/group in triplicate.

among any injection groups or shams, indicating that mitochondria in each group were well coupled.

The use of tGFP-labeled mitochondria allows for visualization and tracking of transplanted mitochondria *in situ*, which is important for determining cell-type incorporation and time lapse uptake of exogenous mitochondria.[46] However, we have also shown that cultured cells can have mitochondria that are well coupled but respire at lower rates.[46] Therefore, we also tested the injection of muscle-derived mitochondria, both as an alternative cell source with different respiratory capacity and as potentially clinically applicable, as autologous transplant may be performed using mitochondria obtained from a muscle biopsy.

Muscle mitochondria were isolated from the soleus muscle of separate naïve rats and then similarly injected into the injured spinal cords. Following transplantation, there was a significant effect in state III respiration (F [4, 21] = 8.714, $p = 0.0003$); post-hoc analyses revealed significant increases with either 50 μg (92% of sham levels) or 100 μg (95% sham levels) mitochondria injection compared with vehicle-injected groups (Fig. 4). There were also significant effects in state V.1 respiration (F [4, 21] = 10.73, $p < 0.000$) and state V.2 respiration (F [4, 21] = 2.977, $p = 0.0429$). Post-hoc analyses showed significant decreases in state V.1 respiration after injury, which was maintained near sham levels with 100 μg mitochondrial transplantation. All injection groups or shams were equally well coupled, as is shown in the RCR values.

The state III OCR results indicate that 100 μg mitochondria transplantation, using either source of mitochondria, maintained oxidative phosphorylation function in the injured spinal cord to ~90% of sham levels. We previously reported that rescue of state III respiration to 67% of sham levels corresponded with long-term tissue sparing and behavioral recovery.[37] Therefore, the 100 μg dosage was used to investigate the effects of mitochondrial transplantation on both cell-type incorporation and long-term recovery.

Characterization of transplanted tGFP mitochondria in situ

We characterized the uptake of exogenous tGFP mitochondria into resident cells of the injured spinal cord. Analysis of multiple time points after injury gave a temporal depiction of exogenous mitochondrial incorporation within tissues after 24 h, 48 h, and 7 days post injection. Injection sites presented as elliptical boluses at the injection epicenter, with scattered punctate labeling further from the injection site (Fig. 1A). Earlier time points showed very discrete injection boluses (Fig. 1B,C), in addition to scattered punctate tGFP mitochondria within the cord (Fig. 1D). By the 7 day time point, these discrete injection boluses were difficult to distinguish, save for in a few instances, and only dispersed punctate tGFP mitochondria were present.

We analyzed the spread of the injected tGFP mitochondria in two ways. The first was a measure of the rostral-caudal distribution of all four injection boluses. There were significant differences in bolus length among time points (F [2, 9] = 22.46, $p = 0.0003$, Fig. 1); post-hoc analysis revealed a significant decrease in bolus length of the 7 day group compared with the 24 and 48 h time points. The length of the bolus appeared to increase, although not significantly, in the 48 h group compared with the 24 h group. We further measured the rostral-caudal length of punctate mitochondria, and found that there were no significant differences among transplantation groups (F [2, 9] = 2.996, $p = 0.1006$) (Fig. 1F). The second analysis was a measure of total volume of injectate throughout the spinal cord (Fig. 1G). The tGFP mitochondria injection bolus volume was significantly different among time points (F [2, 9] = 15.61, $p = 0.001$); post-hoc analysis indicated that the injection did not change volume at either the 24 h or the 48 h time point, but that it decreased volume at the 7 day time point.

All of the tGFP injection sites (four/animal) for the 24 and 48 h groups were visible using fluorescent microscopy. By 7 days post-injection, the injection sites had almost disappeared so that only three total injections across all four animals in the group could be

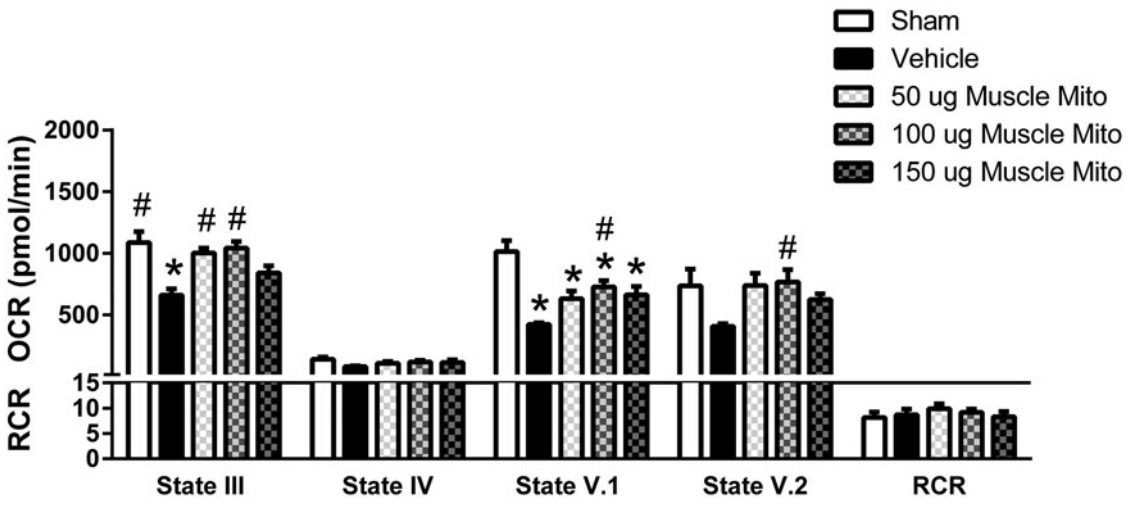

FIG. 4. Muscle-derived mitochondrial (Mito) transplantation maintains respiration rates. State III, V.1 and V.2 oxygen consumption rates (OCR) were maintained near sham levels after 100 μg muscle-derived mitochondrial transplantation. Bars are means ± SEM. *$p < 0.05$ versus sham; #$p < 0.05$ versus vehicle. (One way ANOVA for each state, Tukey's multiple comparison). $n = 4$–6/group in triplicate.

visually verified. Some instances of a remaining injection bolus were still evident, and the rostral-caudal spread of punctate tGFP stippling was similar to that at the 24 and 48 h time points.

We set out to characterize the cell-type-specific co-localization with tGFP mitochondria. We looked at multiple different resident spinal cord cell types when performing our analyses including neurons, brain macrophages, endothelial cells, astrocytes, pericytes, and oligodendrocytes (Fig. 5).

When examining the different cell types within the injection epicenter bolus, we noted an almost complete absence of neurons although there was a high density of brain macrophages. The concentration of mitochondria or the volume of the injections could

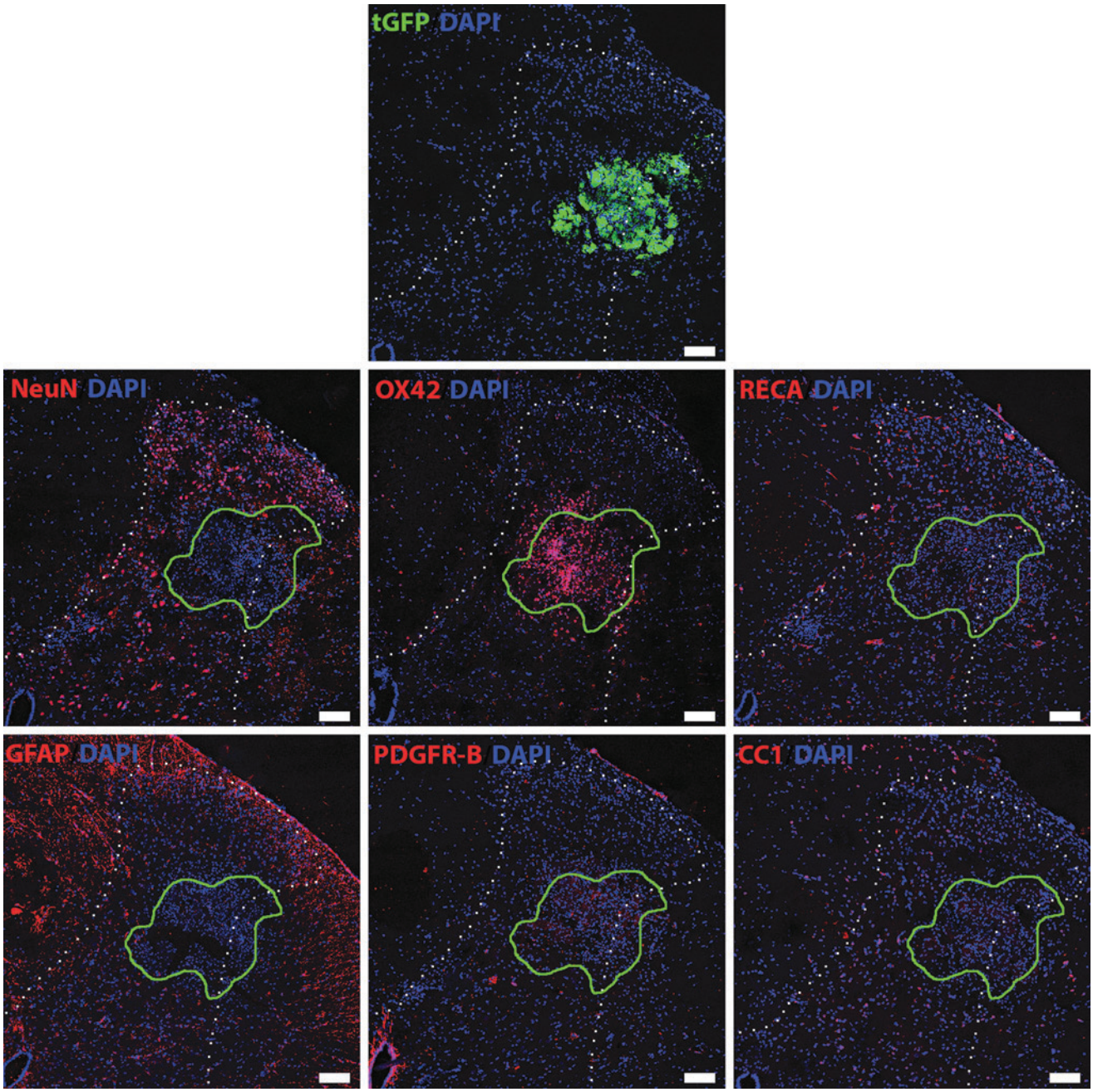

FIG. 5. Resident cell types of the spinal cord proximal to tGFP mitochondrial injection bolus. The top panel shows an injection bolus into the dorsal horn of the spinal cord after 24 h. Adjacent slide series (separated by 40 μM) were stained with specific cell type markers, and the white dotted lines outline the dorsal horn gray matter whereas green lines delineate margins of the injection bolus. Within the injection bolus, there appeared to be a loss of neurons and oligodendrocytes. Although there were few astrocytes within the bolus, they were prevalent in the area surrounding the injection. There was a noticeably increased density of brain macrophages in the area of the injection bolus. Additionally, there were endothelial cells and pericytes seen throughout the injection bolus. tGFP, exogenous tGFP mitochondria; NeuN, neurons; OX42, brain macrophages; RECA, endothelial cells; GFAP, astrocytes; PDGFR-B (platelet-derived growth factor receptor beta), pericytes; CC1, oligodendrocytes; DAPI (4',6-diamidino-2-phenylindole), cell nucleus. Scale bars = 100 μm. Color image is available online at www.liebertpub.com/neu

be damaging the host tissues. When comparing vehicle-injected and tGFP mitochondria-injected spinal cords, there was typically increased brain macrophage activation at the mitochondria injection sites compared with vehicle (Fig. 6A). This indicated that the tGFP mitochondria boluses could be causing inflammatory responses, and semiquantitative analyses of brain macrophage densities within the injection epicenters at different time points (Fig. 6B) showed a significant difference between vehicle- and tGFP mitochondria-injected groups at 24 h ($p = 0.0012$), 48 h ($p = 0.0002$), and 7 days post-injection ($p = 0.0196$).

To discern which cell types incorporated exogenous mitochondria, we quantified incidences of co-localization. Representative images show positive co-localization of various cell types both away from and within the boluses of tGFP injections (Fig. 7), defined in two different ways. The first criterion of positive incorporation was tGFP labeling present within the cytoplasm of the cell, as evidenced by green tGFP labeling within the confines of the red cell membrane marker juxtaposition to the nucleus (DAPI). The second criterion of positive incorporation was when the tGFP labeling overlapped with the cell specific marker, resulting in a yellow signal. If either of these definitions was met, this was counted as a positive instance of co-localization.

We found instances of cell-type specific co-localization with tGFP mitochondria for various cell types including brain macrophages, endothelial cells, pericytes, astrocytes, and oligodendrocytes at 24 h post-transplantation (Fig. 8), with most conspicuous labeling in endothelial cells and perictyes. Co-localization was evident for all cell types both within the injection boluses and more distally, where sparse punctate tGFP was present. However, no evidence of co-localization was found within neurons either within the bolus or distally.

We quantified the propensity of tGFP mitochondria to be incorporated into different cell types spatially with respect to injection sites and across time. Tissue sections were analyzed per hemicord as depicted in the schematic (Fig. 2A), including the two injection epicenters, rostral and caudal to those, and the first section distally that only had punctate tGFP present. To compare propensities for exogenous mitochondrial uptake, from each section we quantified the percentage of a specific labeled cell type within the dorsolateral cross section ROI (Fig. 2B) that was co-localized with tGFP mitochondria.

Comparisons were made to determine which cell type had a higher propensity to incorporate mitochondria. The cell types counted for each of the sections quantified, as described in Figure 2,

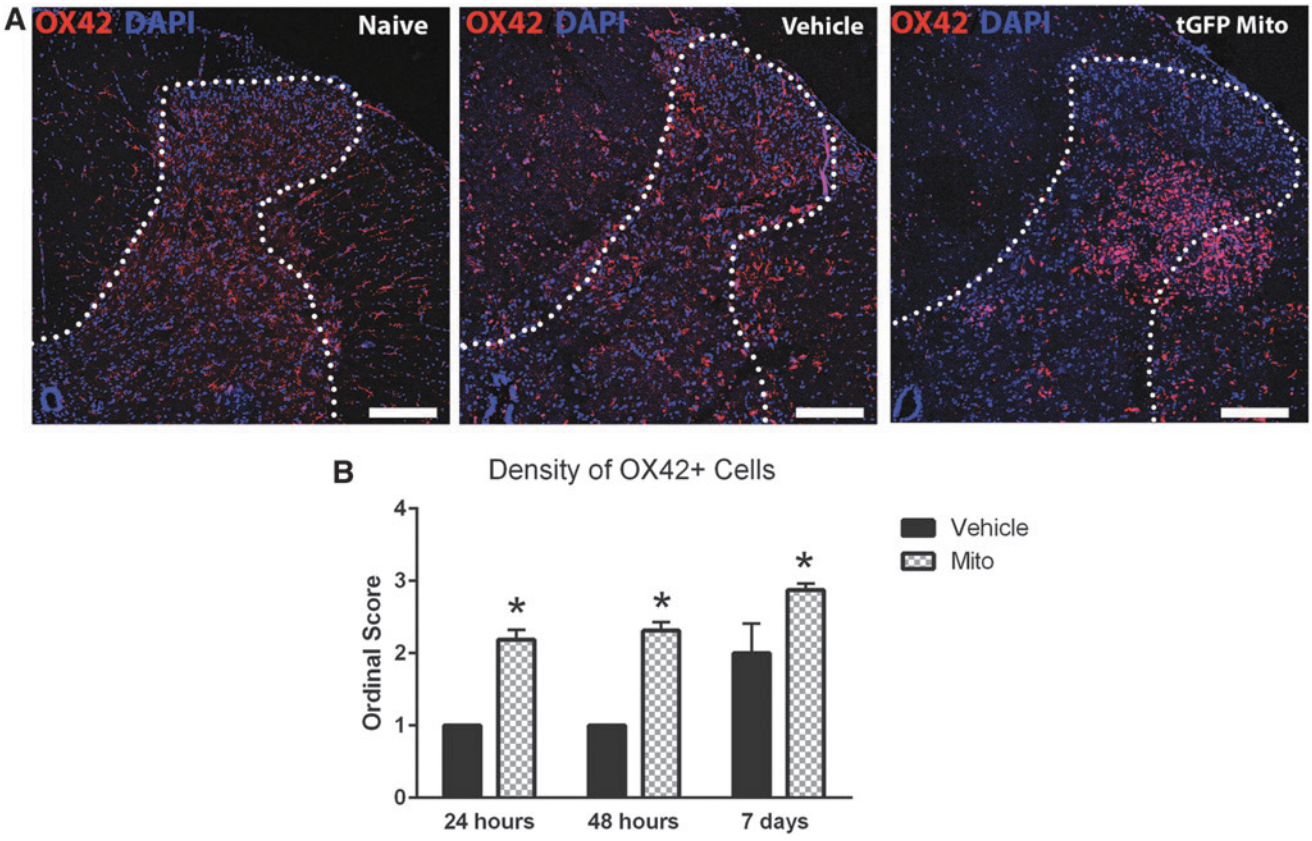

FIG. 6. Brain macrophage activation at the mitochondrial (Mito) injection bolus. **(A)** Microgliosis was compared among naïve, injured/vehicle-injected, and injured/tGFP mitochondria injected spinal cords 24 h after injury. There is a conspicuous high density of brain macrophages within the tGFP injection site compared with vehicle. **(B)** At the injection epicenters, brain macrophage density was given a score of 0–3, where 0 reflects normal quiescent morphologies (**A** naïve) and 3 reflects overt microglial activation and accumulation of brain macrophages. There was a significant increase in the macrophage response when tGFP mitochondria were injected compared with vehicle injections at all time points. Error bars depict median ± SEM. *$p < 0.05$ versus vehicle; (Mann–Whitney *U* test for each time point) $n = 4$ vehicle injections per time point, $n = 16$ tGFP injections per time point. OX42, brain macrophages; DAPI (4',6-diamidino-2-phenylindole), cell nucleus. Scale bars = 200 μm. Color image is available online at www.liebertpub.com/neu

were summed to give a total number per spinal cord (Fig. 9A, white), and instances of co-localization from each of the eight ROI analyzed were totaled (Fig. 9A, black). A one way ANOVA across the total number of cells counted among each specific type showed significant differences at 24 h (F [4, 1] = 72.59, $p < 0.0001$), 48 h (F [4, 15] = 87.46, $p < 0.000$), and 7 days (F [4, 15] = 37.32, $p < 0.0001$). Post-hoc analyses revealed that there were significant differences in the total cell counts among cell types. Interestingly the total brain macrophages counted were significantly higher than all other cell types at each time point. Alternatively, a one way ANOVA showed significant differences among the number of co-localized cells across cell types at 24 h (F [4, 15] = 10.62, $p = 0.000$), 48 h (F [4, 15] = 45.55, $p < 0.0001$), and 7 days (F [4, 15] = 5.159, $p = 0.0081$). Post-hoc analyses showed that co-localization numbers were significantly higher in brain macrophages than all other cell types (Fig. 9A), further depicted in the percentage of cells that co-localized with tGFP (Fig. 9B). A one way ANOVA revealed significant differences between cell type co-localization percentages at 24 h (F [4, 15] = 6.384, $p = 0.0033$) and 48 h (F [4, 15] = 5.854, $p = 0.0048$). Tukey's multiple comparisons showed that both brain macrophages and pericytes co-localized with tGFP at significantly higher rates than oligodendrocytes at 24 and 48 h post-injection, which had the lowest co-localization percentages at any time point.

The injection epicenters contained dense boluses of tGFP mitochondria, and based on the high concentrations in this area, it may be difficult for mitochondria to have access to various host cells for incorporation. Notably, sections that were further from the injection epicenters showed highly dispersed tGFP mitochondria that may have differential uptake, because higher concentrations of mitochondria have been shown to aggregate with less extensive distribution into nearby brain tissues in a rat model of Parkinson's disease.[57] We therefore mapped the propensity of co-localization in relation to the injection epicenters, as described, and analyzed this across the rostral-caudal distribution of all the sections analyzed for each spinal cord (Fig. 10).

Two way ANOVAs were performed within time points for each cell type and showed differences in cell-type co-localization for macrophages (F [2, 9] = 8.123, $p = 0.0096$), endothelial cells (F [2, 9] = 10.69, $p = 0.0042$), oligodendrocytes (F [2, 9] = 9.575, $p = 0.0059$), astrocytes (F [2, 9] = 22.54, $p = 0.0003$), and pericytes (F [2, 9] = 928.3, $p < 0.0001$). We found that co-localization percentages depended upon their location in relation to the injection epicenters, especially at the 24 h time point when macrophages had higher incorporation percentages one section rostral of each injection site (400 μm) compared with the most caudal section analyzed. Endothelial cells and astrocytes had higher co-localization percentages closer to the injection epicenters compared with the distal sections, whereas pericytes tended to have more stable co-localization across sections. Oligodendrocytes had very low incorporation percentages, with the least incorporation

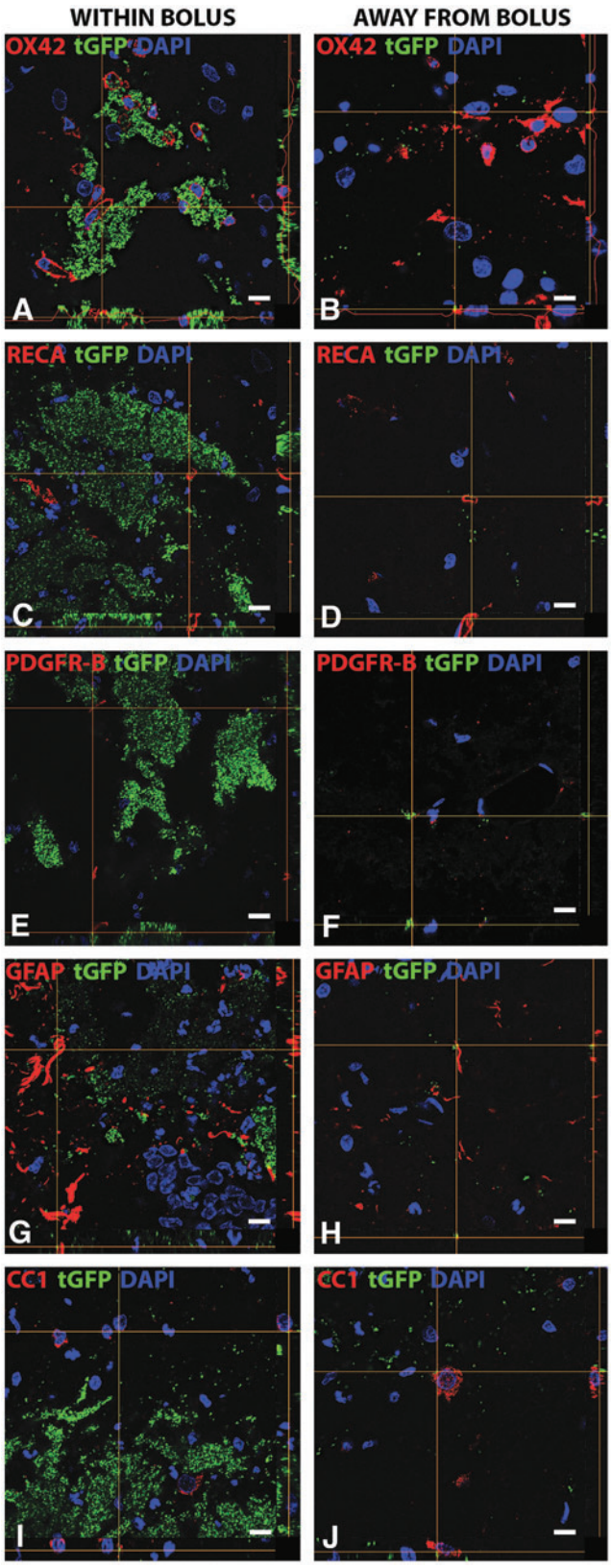

FIG. 7. Representative images of cell type-specific tGFP co-localization. Co-localization with different cell types at 24 h post-injury in captured Z-stack images with the bottom panel of each image representing the x plane and the right panel representing the y plane. "Within Bolus" (left column) indicates images that were taken in the area of dense tGFP mitochondria, whereas "Away from Bolus" (right column) indicates images that were taken in areas with more sparse, punctate tGFP mitochondria. Co-localization was evident within macrophages **(A, B)**, endothelial cells **(C, D)**, pericytes **(E, F)**, astrocytes **(G, H)**, and oligodendrocytes **(I, J)**. OX42, brain macrophages; RECA, endothelial cells, PDGFR-B (platelet-derived growth factor receptor beta), pericytes, GFAP, astrocytes; CC1, oligodendrocytes; tGFP, exogenous tGFP mitochondria; DAPI (4',6-diamidino-2-phenylindole), cell nucleus. Scale bars = 10 μm. Color image is available online at www.liebertpub.com/neu

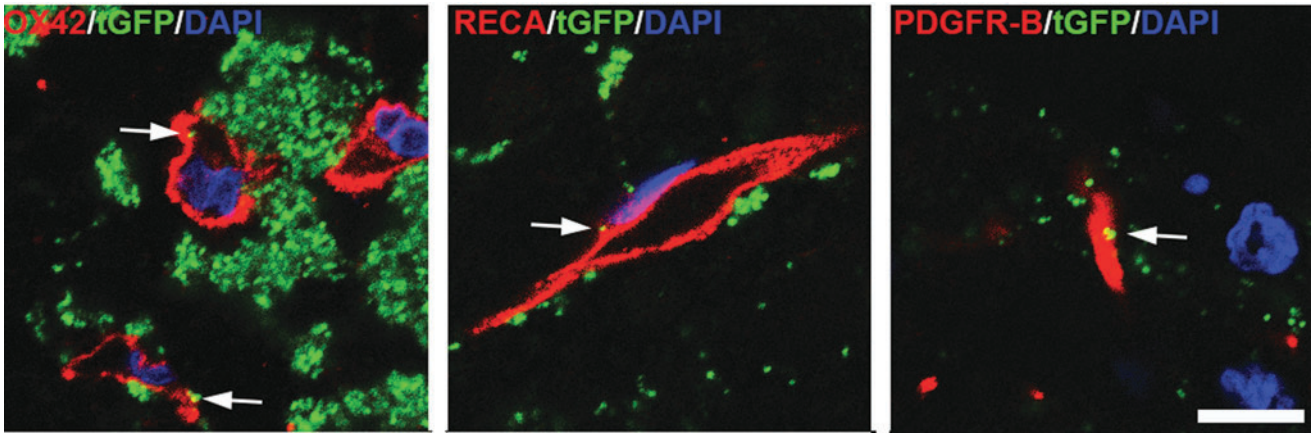

FIG. 8. High magnification images showing positive co-localization. Images show instances of cell-type specific co-localization of tGFP mitochondria with macrophages, endothelial cells, or pericytes. White arrows point to instances of tGFP mitochondria co-localization within the cells. Tissues were processed 24 h post-tGFP mitochondria transplantation. OX42, brain macrophages; RECA, endothelial cells; PDGFR-B (platelet-derived growth factor receptor beta), pericytes; tGFP, exogenous tGFP mitochondria; DAPI (4',6-diamidino-2-phenylindole), cell nucleus. Scale bar = 10 μm. Color image is available online at www.liebertpub.com/neu

distal to the injection epicenters. This indicates spatial-dependent incorporation in addition to cell-type dependent incorporation.

We also performed morphometric analyses to examine possible changes in lesion volume or tissue sparing at acute time points after injury (Fig. 11). Overall, there were no apparent changes in lesion volume, gray matter sparing, or white matter sparing.

Behavioral recovery and tissue sparing after mitochondrial transplantation

We tested the effects of mitochondrial transplantation after SCI on hindlimb functional recovery and tissue sparing. Anesthetized animals underwent a severe contusion injury at the L1/L2 spinal

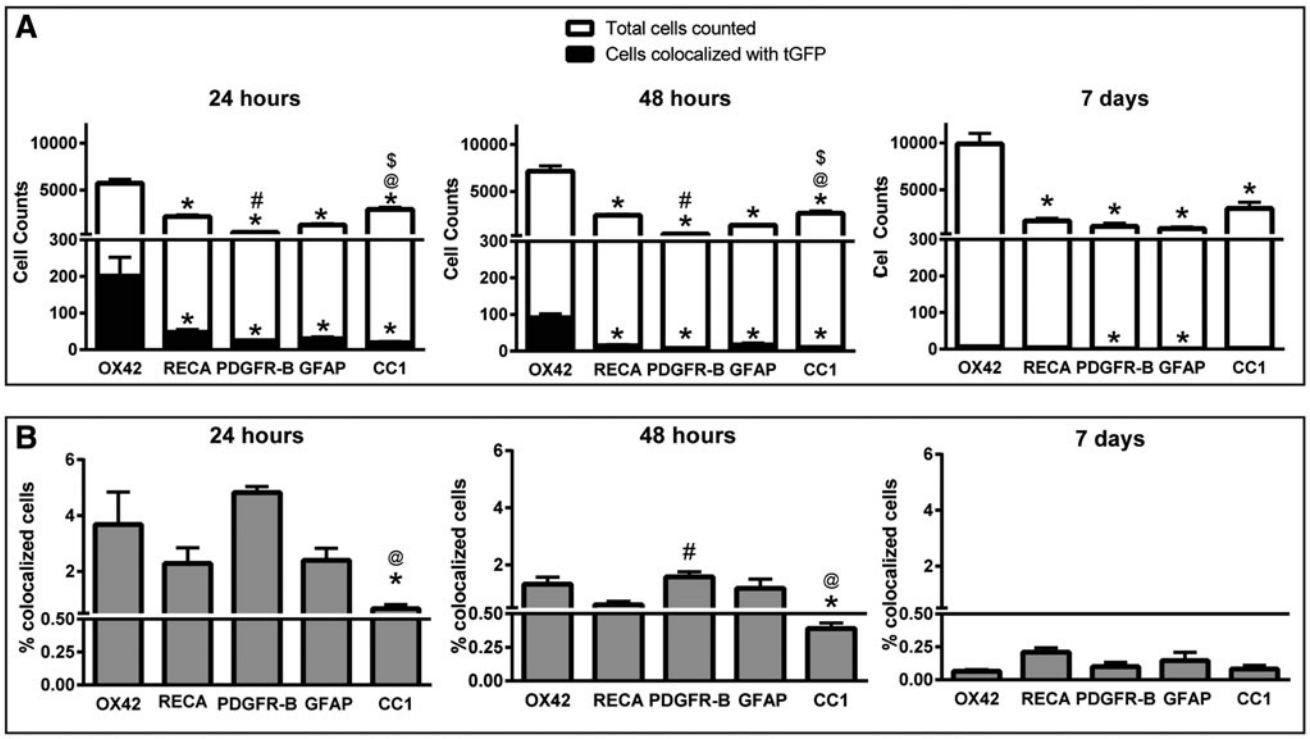

FIG. 9. Cell-type co-localization of tGFP mitochondria across time. **(A)** Total numbers of a given cell type were counted (white bars), as well as the number of cells co-localized with tGFP (black bars) for all regions of interest (ROI) analyzed per spinal cord. **(B)** Cell type co-localization was calculated as a percentage of total cells that had tGFP. Brain macrophages and pericytes had significantly higher co-localization percentages than oligodendrocytes at 24 and 48 h. There were no differences in percent co-localization among cell types at 7 days. OX42, brain macrophages; RECA, endothelial cells; PDGFR-B (platelet-derived growth factor receptor beta), pericytes; GFAP, astrocytes; CC1, oligodendrocytes; tGFP, exogenous tGFP mitochondria. *$p < 0.05$ versus OX42; #$p < 0.05$ versus RECA; @$p < 0.05$ versus PDGFR-B; \$$p < 0.05$ versus GFAP (one way ANOVA, Tukey's multiple comparisons) $n = 4$/group. Bars are means ± SEM.

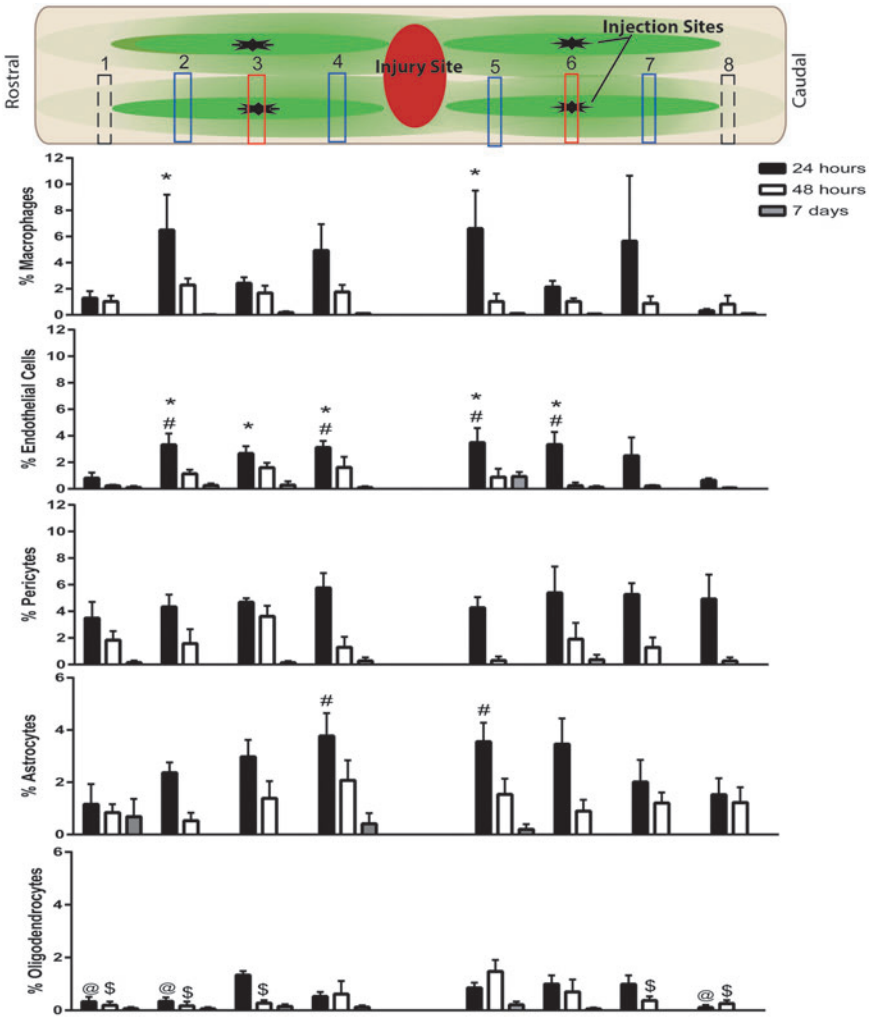

FIG. 10. Rostral-caudal cell-type incorporation of tGFP mitochondria over time. Co-localization was quantified within regions of interest (ROIs) across eight different sections (numbered 1–8) in relation to injection epicenters. Top panel schematic of counted sections corresponds to the rostral-caudal counts of co-localization percentages at both injection epicenters (red boxes), sections 400 μm rostral and 400 μm caudal to the injection epicenters (blue boxes), and the first section where only punctate tGFP mitochondria were present (dashed black boxes). There were differences in co-localization percentages among location sites when analyzed within cell types. *$p < 0.05$ versus section 8; #$p < 0.05$ versus section 1; @$p < 0.05$ versus section 3; \$$p < 0.05$ versus section 5 (two way repeated measures ANOVA, Tukey's multiple comparisons) $n = 4$/group. Bars = mean ± SEM. Color image is available online at www.liebertpub.com/neu

level, followed immediately by four injections for a total of 100 μg tGFP-labeled mitochondria into the injury penumbra (see Fig. 1A for injection schematic).

The starting number per experimental group was 12. Through the course of the 6 week long study, we observed an attrition of animals typical of SCI studies. Three animals died from anesthesia during surgical procedures, three animals were removed from the study and euthanized because of extensive autophagia (self-cannibalism or chewing and biting of tissue) of the hindlimbs, and one animal was removed from the study because of its high 2 day BBB score (> 2 SD from the mean, indicating a bad contusion injury). This resulted in final groups of vehicle injection ($n = 10$), tGFP mitochondria injection ($n = 11$), and muscle mitochondria injection ($n = 8$).

Animals were tested for mechanical sensitivity of the hindpaws with the von Frey hair test and for hindlimb motor recovery with the overground locomotor BBB scale. Within 3 weeks of injury, we observed the development of mechanical hypersensitivity in all groups (Fig. 12A). Mitochondria transplant produced an extended duration of hypersensitivity to at least 6 weeks post-injury, as compared with all other groups. A two way ANOVA revealed a main effect of time (F [2, 52] = 17.64, $p < 0.0001$) but not treatment (F [2, 26] = 1.370, $p = 0.2718$). Post-hoc analyses showed that each treatment group had significantly decreased scores at 3 weeks compared with their within-group baseline levels, indicating potentially increased hypersensitivity. As indicated earlier, three animals were removed for the study because of extensive autophagia. After experiments were completed and the data were analyzed, the study was unblended, which revealed that these animals had all been in the muscle mitochondria transplanted group.

A two way repeated measures ANOVA revealed no effect of treatment on BBB scores (F [2, 26] = 0.01894, $p = 0.981$) (Fig. 12B). All animals showed some functional recovery consistent with our previous studies.[37] The injured rats in the current studies plateaued with an average BBB score of ~8, which is indicative of hindlimb sweeping and plantar placement without weight bearing.[48] This level of recovery correlates to historical data using this injury severity and

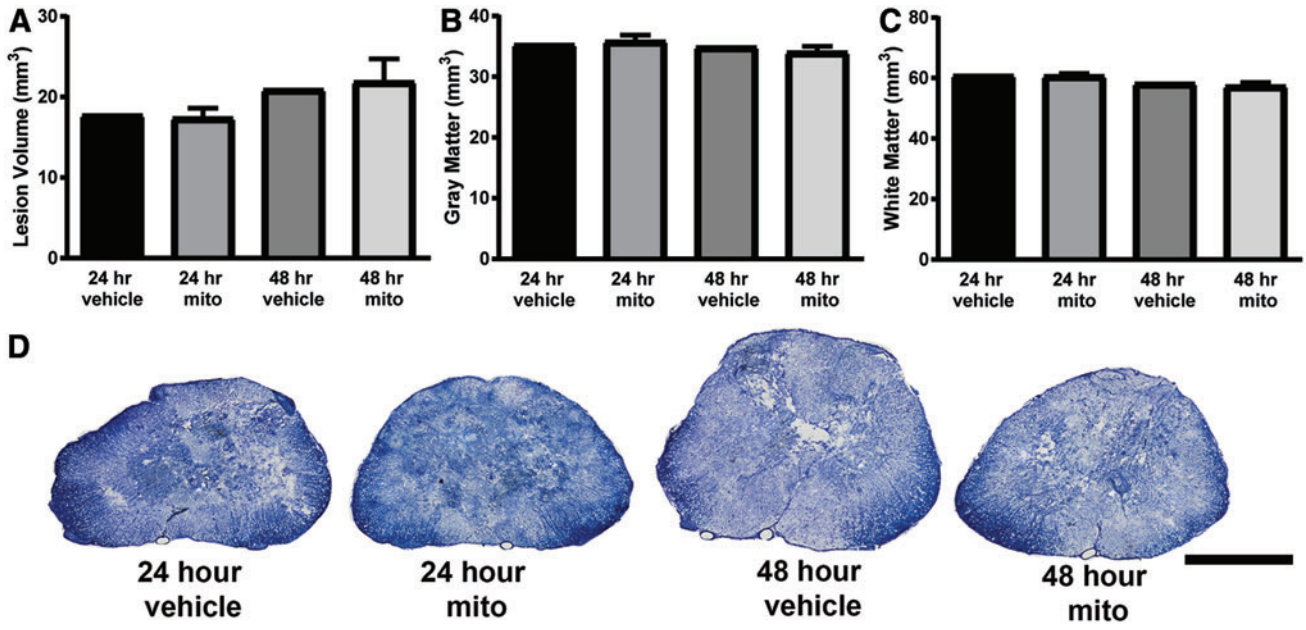

FIG. 11. Histological assessments of tissue sparing at acute time points. Lesion volume **(A)**, gray matter sparing **(B)**, and white matter sparing **(C)** showed no apparent differences. Representative images show no apparent differences in tissue sparing at the injury epicenter among groups **(D)**. $n = 1$ vehicle; $n = 4$ mitochondria (mito) per time point. Bars = mean ± SEM, Scale = 1 mm for histological photos. Color image is available online at www.liebertpub.com/neu

spinal level, indicating there was no overt damage/effect of injections volumes. It is important to note that although we did not see improvements in functional recovery with mitochondrial transplantation, there was no further impairment of function, which had been a concern, based on possible increased inflammatory responses.

Following terminal behavioral analyses, animals were euthanized and spinal cords were processed for tissue sparing analyses that showed similar histopathology among treatment groups, supporting behavioral findings (Fig. 13). There were no significant differences among groups for lesion volume (Fig. 13A). Mitochondria injections were targeted to the medial lateral gray matter, allowing for possible mitochondrial integration into both gray matter and white matter; however, there were no differences among treatment groups for either gray matter or white matter tissue sparing (Fig. 13B and C, respectively).

Our previous documentation of improved functional recovery after treatment with an alternative mitochondria biofuel (ALC) was highly correlated with significant sparing of putative CPG interneurons rostral to the SCI.[37] Despite there being no behavioral differences, we investigated similarly whether mitochondrial

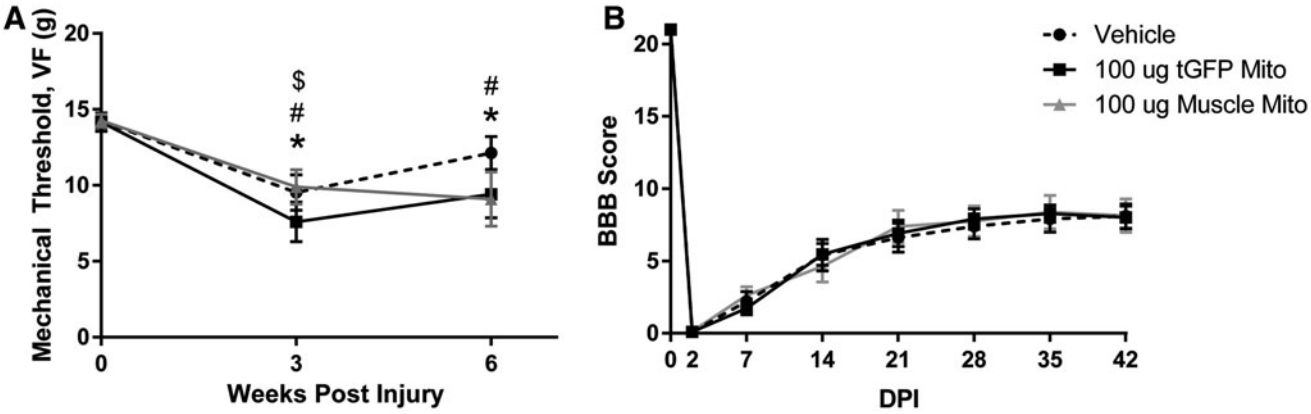

FIG. 12. Hindlimb sensitivity and functional recovery after spinal cord injury (SCI) and mitochondrial (Mito) transplantation. **(A)** Mechanical hypersensitivity following SCI and mitochondrial transplantation. Mitochondrial transplantation extended the duration of mechanical hypersensitivity after SCI. SCI similarly decreased mechanical threshold in all groups at 3 weeks after SCI. At 6 weeks post-injury, however, mechanical thresholds in the vehicle-injected and tGFP mitochondria-injected animals returned toward baseline levels, whereas those in the muscle mitochondria transplanted group remained significantly lower. **(B)** Basso, Beattie, Bresnahan (BBB) scores for all animals were significantly decreased after SCI, with gradual increases over time after injury, although there were no significant differences among treatment groups. DPI, days post-injury. Bars are means ± SEM. $\$p < 0.05$ vehicle versus baseline vehicle; $*p < 0.05$ tGFP mito versus baseline tGFP mito; $\#p < 0.05$ muscle mito versus baseline muscle mito (two-way repeated measures ANOVA, Tukey's multiple comparisons) $n = 8$–11/group.

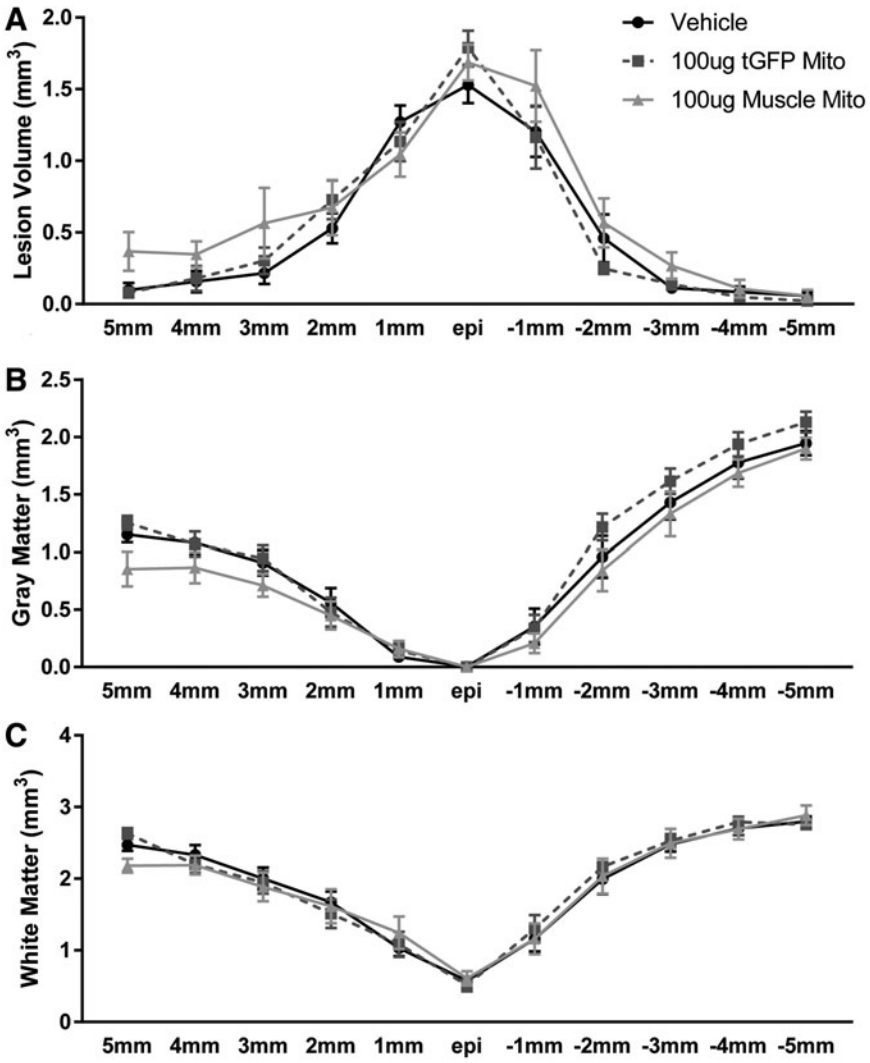

FIG. 13. Tissue sparing analyses 6 weeks after injury and mitochondrial (Mito) transplantation. At 6 weeks post-injury and injection, morphometric analyses were performed to find no differences among groups for total lesion volume **(A)**, or for gray matter **(B)** or white matter **(C)** sparing at different spinal cord levels in relation to the injury epicenter. Bars are means ± SEM. (Two way ANOVA) $n = 8–11$/group.

transplantation spared interneurons by performing stereology after injury and transplantation (Fig. 14). We defined the ROI for neuronal counts to include lamina X and the central portion of lamina VII (Fig. 14A).

The number of neurons estimated in each section was extrapolated using a previously published equation.[58] The coefficient of error (CE) (vehicle, 0.116; tGFP mitochondria, 0.1126; muscle mitochondria, 0.1456) and coefficient of variance (CV) (vehicle, 0.7007; tGFP mitochondria, 0.6506; muscle mitochondria, 0.5145) were calculated for each group to establish intra- and inter-animal variation, respectively. There were significant differences in neuronal sparing among groups (F [2, 286] = 3.658, $p = 0.0270$), and post-hoc analyses showed significantly more neurons at 1 mm caudal to the injury epicenter in the tGFP mitochondria-injected groups than in both vehicle- and muscle mitochondria-injected groups.

Discussion

The current study is the first to assess mitochondrial transplantation into the injured rat spinal cord and its effects on bioenergetics at 24 h post-injury/transplantation, as well as long-term behavior and histology. We found that injections of both tGFP labeled culture-derived and muscle-derived mitochondria significantly maintained state III respiration at the 100 μg dosage compared with vehicle injections. We have previously shown that pharmacologically maintaining state III respiration near sham levels after L1/L2 SCI results in functional neuroprotection.[37] Accordingly, both sources of isolated mitochondria were injected at 100 μg to evaluate the effects of mitochondrial transplantation on host cellular uptake acutely, as well as long-term histological and behavioral outcome measures.

Mitochondrial incorporation into host cells

We first assessed the time course of exogenous tGFP mitochondrial incorporation into host cells. Discrete tGFP mitochondria boluses were evident at 24 and 48 h, although they decreased significantly in volume and rostral-caudal spread by 7 days post injection. There are likely various reasons for the scarcity of tGFP label at 7 days (and 6 weeks) after injection, notably phagocytosis, especially at the injection site bolus where the mitochondria density may be too high to be incorporated into the surrounding host cells.[57] The tGFP mitochondria within the extracellular space likely diffuse

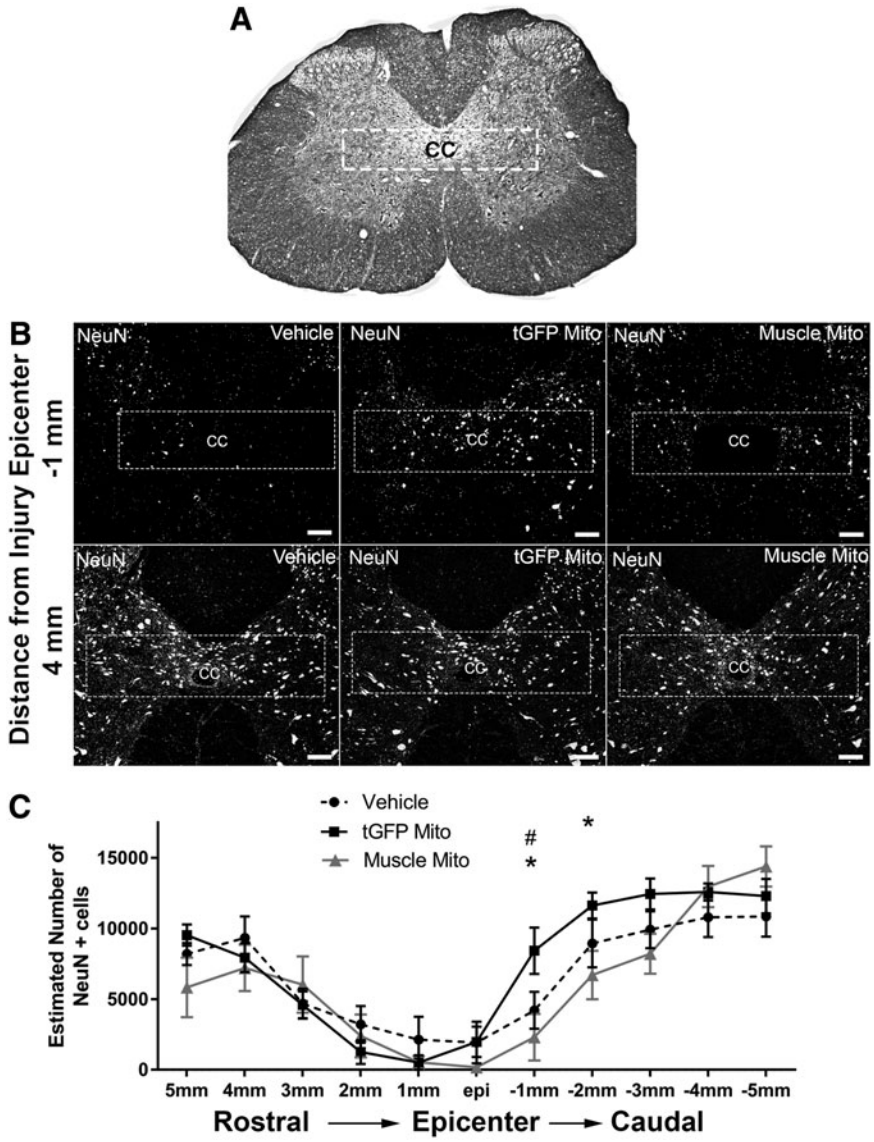

FIG. 14. Neuronal counts in the upper lumbar spinal cord after injury. **(A)** Eriochrome cyanine-cresyl violet (ECCV) stained section of the spinal cord showing the region of interest (ROI) analyzed including lamina X and part of lamina VII, which include putative central pattern generator neurons. CC, central canal. **(B)** Representative images showing neurons in the ROI (dashed boxes) at 4 mm rostral and −1 mm caudal of the injury epicenter. There appeared to be more NeuN staining within the ROI of the mitochondria-injected animals at 1 mm caudal to the injury compared with either vehicle- or muscle mitochondria (Mito)-injected groups. **(C)** Stereological counts were performed on 11 equally spaced spinal cord sections, centered on the injury epicenter (epi). Each point on the graph is the estimated number of NeuN-positive cells within subvolumes of spinal cord separated by 1 mm length. NeuN-positive cells were significantly higher in tGFP mitochondria-injected groups than in the other cohorts at 1 mm caudal to the injury epicenter, and also significantly higher than muscle mitochondria groups at 2 mm caudal to the injury epicenter. Bars are means ± SEM. $*p < 0.05$ tGFP mito versus muscle mito; $\#p < 0.05$ tGFP mito versus vehicle, (two way ANOVA, Tukey's multiple comparisons) $n = 8$–11/group.

easily through tissues away from the injection site over time, especially in the white matter where there is greater longitudinal diffusion. Moreover, when tGFP mitochondria successfully incorporate into cells, they may fuse and divide with host cell mitochondria leading to a wider dispersal of tGFP fluorescent within cells. Conversely, others have reported evidence of fluorescently labeled mitochondria at chronic time points. In a porcine model of cardiac ischemia using direct mitochondrial transplantation and an antibody against human mitochondria, the presence of exogenous human mitochondria was shown 4 weeks after injection.[59] This method of labeling, however, was not dependent on the retention of a fluorescent tag that was present at the time of injection; that is, the tGFP tag, and instead used antibodies to label a different species-derived mitochondria *in situ*. Alternatively, GFP-labeled mitochondria conjugated with the peptide carrier protein, Pep-1, and when directly injected into rat brains in a Parkinson's disease model, were observed in the medial forebrain bundle 12 weeks after injection.[57]

Differences in cell-type incorporation

We also evaluated the propensity of tGFP mitochondria incorporation into various cell types and revealed that brain macrophages

and pericytes had the highest propensity to co-localize with exogenous mitochondria. We cannot discern, however, whether the tGFP mitochondria were functionally incorporated within macrophages or if they had been degraded and phagocytosed. Alternatively, pericytes are found within the vascular basement membrane and are closely associated with endothelial cells with many similarities to macrophages, including mesodermal origin, possessing of lysosomes, similar cell surface markers, and prostaglandin secretion (for review on central nervous system [CNS] pericytes see studies by Muramatsu and Yamashita, Winkler and coworkers, and Armulik and coworkers[60–62]). Further, these cells have contractile properties and can regulate capillary diameter, making them influential in vascular perfusion of the spinal cord, especially after injury.[63] These traits may explain their high propensity to co-localize with exogenous mitochondria, although as with macrophage co-localization, we cannot definitively say at this time if the mitochondria were phagocytosed or incorporated functionally into the cells. Oligodendrocytes were least co-localized with tGFP mitochondria, although this could possibly be the result of the location of the injection sites more targeted to the gray matter. Although tGFP mitochondria co-localized with variety of cell types, it is important to note that they were conspicuously absent in neurons. There was conspicuous neuronal loss in the dorsal gray matter where injection boluses were located (Fig. 5), which may be the result of multiple factors. High concentrations of mitochondria can result in aggregation of the mitochondria, further making it difficult to incorporate into cells. These aggregations could physically injure neuronal cells as well as cause a heightened inflammatory response. This, in addition to the volume of fluid injected, could disrupt the tissue. We have noted that injection volume of vehicle alone activated brain macrophages. The white matter of the spinal cord is more amenable to fluid diffusion along axons. In gray matter where cell bodies are more compactly arranged, injected fluids could cause more physical stress even with the slow injection rates. Therefore, a balance must be attained that allows for low enough concentration of mitochondria that there is minimal aggregation, but also low total volume injected to avoid tissue damage. Additionally, a delivery method in which the mitochondria are somehow encapsulated may be a defining feature necessary for incorporation into neurons, as was used in previous studies utilizing mitochondria transplant in stroke.[43] It is important to note, however, that if other cell types in the injury penumbra can be spared following mitochondrial transplantation, then the inhospitable environment may be more favorable for neuroprotection. For example, salvaging pericytes and endothelial cells could increase perfusion of the spinal cord, thus being overall protective indirectly of neuronal survival.

Long-term outcome measures

Despite significant effects on injured tissue bioenergetics acutely, we found that the same transplantation paradigm used in long-term studies did not result in reciprocal restoration of hindlimb locomotion or sensory tactile thresholds or tissue sparing. As expected, contusion SCI significantly decreased BBB locomotor scores for each group, with characteristic spontaneous functional recovery that plateaued 5 weeks post-injury consistent with severe injury at the L1/L2 spinal level.[17] Transplantation of mitochondria from either source did not increase or hamper this recovery. An important consideration is the origin of the donor mitochondria. The current experiments utilized mitochondria isolated from cultured PC-12 cells or soleus muscle tissue. Mitochondrial respiration and function can vary dependent upon the source.[64] Here, we used a mitochondrial origin similar to the recipient species (rat), and we compared two different tissue source types. Future studies and characterizations comparing donor tissues with different mitochondrial respiratory activities may establish sources that are more beneficial in our trauma/transplantation paradigm. Determining the compatibility of injected mitochondria with host cell mitochondrial networks may reveal that autologous transplantation has different effects than syngeneic or xenogeneic sources.

Contusion SCI also decreased mechanical sensitivity thresholds in each group, with some recovery toward baseline. However, mitochondrial transplantation increased, rather than decreased, the duration of this hypersensitivity, indicating possibly enhanced central neuropathic pain. Morphometric analyses in relation to the injury epicenter were consistent with the BBB outcome measures, showing no significant group differences in the rostral-caudal extent of lesion volume or spared gray and white matter volumes. Interestingly, however, cell counts showed significantly higher numbers of interneurons in the dorsal gray commissure 6 weeks after tGFP mitochondria injections compared with vehicle or muscle-derived mitochondria, although this was only evident 1–2 mm caudal to the injury epicenter. Nevertheless, although these differences were significant, it did not result in changes in locomotor recovery. This is in diametric contrast to our documentation that sparing of dorsal gray commissure interneurons rostral to the injury epicenter following treatment with the alternative mitochondrial biofuel, ALC, correlated with significant functional improvement in hindlimb function and tissue sparing in the same injury model.[37,65]

Our behavioral (BBB) findings are in agreement with those of Magnuson and coworkers[65] showing that kainic acid depletion of hindlimb CPG neurons with caudal gray matter sparing after contusion SCI does not result in improved BBB scores. This indicates that critical interneurons comprising the CPG located at the L1/L2 spinal level in rats were not spared with mitochondrial treatment, notably those rostral to the injury epicenter that appear critical for functional improvements. These neurons mediate rhythmic output to motor neurons of the lumbar enlargement; therefore, had we found sparing of interneurons cells rostral to the injury, we might have seen BBB improvements, as in previous reports.[37,65]

Addressing potential inflammatory responses

Our findings show the feasibility of mitochondrial transplantation into injured spinal cord tissue and the ability to maintain acute bioenergetics. There are multiple caveats to consider as to why this did not correspond to improved long-term functional outcome measures. We noted that the influx of brain macrophages into the injection sites appeared enhanced in the mitochondrial transplantation group, although this did not alter overall tissue sparing at all acute and long-term time points. The mitochondria we assessed included both endogenous host mitochondria as well as injected mitochondria; therefore, those from accumulating brain macrophages were included in, and may have contributed to results of, our bioenergetics assays. The volume of vehicle or tGFP mitochondria injections likely disturbs the surrounding spinal cord tissue causing nominal injury and subsequent influx of macrophages. Further, mitochondria are a source of damage-associated molecular patters (DAMPS)[66] that can elicit stronger immune responses than vehicle alone. Thus, the consequent accumulation of brain macrophages after mitochondrial injections may have increased the overall number of respiration-competent cells in injury sites evaluated. Although the noted focal cellular immune responses did not alter acute and long-term histopathology or long-term overground locomotion, mitochondrial transplantation prolonged the duration of hindlimb hypersensitivity after SCI. Hypersensitivity in the

muscle-derived mitochondria transplant group may have contributed to noted attrition caused by autophagia, but whether enhanced local inflammatory responses contributed is uncertain.

On the contrary, previously published studies investigating mitochondrial transplantation that tested for inflammatory markers did not find increases. Masuzawa and coworkers found that after direct autologous mitochondria injection into cardiac tissue, there was significantly decreased expression of tumor necrosis factor α, interleukin 6, and high-sensitivity C-reactive protein.[40] Further, they did not find antimitochondrial antibodies present in blood serum samples 28 days after injections. However, there could be differences when allogeneic mitochondria are transplanted, as in our study, compared with a syngeneic or autologous mitochondrial transplant; and into the injured spinal cord.

Possible caveats and future directions

Although there was no apparent integration of transplanted mitochondria into resident neurons, their incorporation into other cell types should not be discounted. The spinal cord is a heterozygous mixture of different cell types, each with important characteristics for the overall health and function of the spinal cord. Macrophages can be either pro-inflammatory or anti-inflammatory, and are responsible for phagocytosing debris and foreign substances as well as having a part in mediating immune response.[67] Astrocytes are important support cells for neurons, help maintain the blood–brain barrier, and perform functions in ion homeostasis of extracellular fluids.[68] Oligodendrocytes play an imperative role in insulating axons to increase signal transmission efficiency.[69] Endothelial cells supply blood and oxygen to tissues, and pericytes wrap around endothelial cells for contraction of vessels and regulation of blood flow.[70] Each of these cell types have important roles in maintaining homeostasis within spinal cord tissues, and salvaging any of these cell types with healthy mitochondrial delivery could be beneficial for functional recovery and neuronal cell survival after SCI.

There is the unconventional possibility that transplanted mitochondria exert their effects extracellularly. The McCully laboratory noted functional benefits of cardiac tissue mechanics after ischemia/reperfusion injury was followed by direct mitochondrial injections.[7,40] Similar to in our studies, they noted a low incorporation rate into host cells and theorized that their results were attributed to extracellular functions of the transplanted mitochondria. If mitochondria can function extracellularly, then it can be reasoned that this would be short lived before immune responses and debris-clearing mechanisms are enacted to remove them, and may therefore explain our short-term benefits without corresponding long-term correlates.

Our recent studies *in vitro* show that co-incubation alone was sufficient for tGFP mitochondria uptake into cultured cells.[46] Similarly, we show here that direct injection of isolated mitochondria into spinal cord tissue *in vivo* results in cellular uptake, although there is a relatively low incorporation rate ($\sim \leq 6\%$ for any specific cell type analyzed). Increasing incorporation efficiency after SCI may be a critical step toward making such transplantation approaches successful in achieving long-term recovery goals. Multiple mechanisms of exogenous mitochondrial incorporation have been proposed, although there is currently no consensus whether it is endocytosis mediated or much more complicated.[71]

Mitochondrial uptake is reported following co-incubation with cells *in vitro* [72,73] or into host cells after direct injection *in vivo*.[7,59] Conjugation of mitochondria with Pep-1, a cell-penetrating peptide that increases incorporation, further promotes mitochondrial uptake,[45,57,74] and connexins or gap junction-mediated communication appears necessary for cells to take in extracellular mitochondria,[75–77] perhaps via actin-dependent processes.[41] Because mitochondria are theorized to be bacterial in origin, and various bacteria up to 5 μm in size can enter cells and replicate, we posit here that similar mechanisms may be used to incorporate isolated mitochondria 500 nm in size. Bacteria can have surface proteins that bind to receptors located on host cells, subsequently initiating zipper-like actin-mediated phagocytosis. As mitochondria are bacterial in origin, and have retained their own set of mitochondrial DNA that encodes for proteins, it is possible then that mitochondria may have the same or similar surface proteins that can bind to cellular receptors. If mitochondria do indeed utilize the zipper-like actin-mediated phagocytosis method of cellular entry, this theory would support others' findings that mitochondrial incorporation is actin dependent. The zipper-like mechanism of bacterial incorporation can utilize different receptors such as integrins for binding and signaling (for review of bacterial invasion methods see the study by Muramatsu and Yamashita[60]). Internalization of exogenous mitochondria-containing particles *in vivo* is reported to be dependent upon integrin-mediated Src/spleen tyrosine kinase (Syk) signaling,[43] further implicating the zipper-like method of internalization as the means for exogenous mitochondrial incorporation *in vivo*. Further in-depth comparisons are needed to determine if mitochondria contain surface proteins that can be responsible for binding and infiltration of host cells.

Although our findings of acute maintenance of cellular respiration are promising, perhaps assessing acute bioenergetics is not the optimal criterion for predicting long-term functional recovery in mitochondrial transplant paradigms after SCI. Accordingly, further investigations of other biomarkers and/or outcome measures of recovery at the more acute time points within the 1st week after injury appear necessary. Herein we show the feasibility of mitochondrial transplantation after SCI, although important caveats such as incorporation mechanism and mitochondrial viability and functional integration remain unanswered. Consequently, this seminal study advances the burgeoning field of mitochondrial transplantation and lays the foundation for increasing incorporation efficiency and cell-type targeting that may be key in improving long-term nfunctional neuroprotection in models of SCI.

Acknowledgments

This study was supported by National Institutes of Health (NIH) F31 NS093904-01A1 (J.L.G.), Conquer Paralysis Now (A.G.R.), NIH R21 NS096670 (A.G.R.), Spinal Cord and Brain Injury Research Center (SCoBIRC) Chair Endowment (A.G.R.), and NIH/National Institute of Neurological Disorders and Stroke (NINDS) 2P30NS051220.

Author Disclosure Statement

No competing financial interests exist.

References

1. Dumont, R.J., Okonkwo, D.O., Verma, S., Hurlbert, R.J., Boulos, P.T., Ellegala, D.B., and Dumont, A.S. (2001). Acute spinal cord injury, part I: pathophysiologic mechanisms. Clin. Neuropharmacol. 24, 254–264.
2. Rowland, J.W., Hawryluk, G.W., Kwon, B. and Fehlings, M.G. (2008). Current status of acute spinal cord injury pathophysiology and emerging therapies: promise on the horizon. Neurosurg Focus 25, E2.
3. Mizuno, Y., Ohta, S., Tanaka, M., Takamiya, S., Suzuki, K., Sato, T., Oya, H., Ozawa, T. and Kagawa, Y. (1989). Deficiencies in complex I subunits of the respiratory chain in Parkinson's disease. Biochem Biophys Res Commun 163, 1450–1455.

4. Winklhofer, K.F., and Haass, C. (2010). Mitochondrial dysfunction in Parkinson's disease. Biochim. Biophys. Acta 1802, 29–44.
5. Swerdlow, R.H., and Khan, S.M. (2004). A ''mitochondrial cascade hypothesis'' for sporadic Alzheimer's disease. Med Hypotheses 63, 8–20.
6. Lin, M.T., and Beal, M.F. (2006). Mitochondrial dysfunction and oxidative stress in neurodegenerative diseases. Nature 443, 787–795.
7. McCully, J.D., Cowan, D.B., Pacak, C.A., Toumpoulis, I.K., Dayalan, H., and Levitsky, S. (2009). Injection of isolated mitochondria during early reperfusion for cardioprotection. Am. J. Physiol. Heart Circ. Physiol. 296, H94–H105.
8. Ide, T., Tsutsui, H., Hayashidani, S., Kang, D., Suematsu, N., Nakamura, K., Utsumi, H., Hamasaki, N., and Takeshita, A. (2001). Mitochondrial DNA damage and dysfunction associated with oxidative stress in failing hearts after myocardial infarction. Circ. Res. 88, 529–535.
9. Bolanos, J.P., Moro, M.A., Lizasoain, I., and Almeida, A. (2009). Mitochondria and reactive oxygen and nitrogen species in neurological disorders and stroke: therapeutic implications. Adv. Drug Deliv. Rev. 61, 1299–1315.
10. Krajewski, S., Krajewska, M., Ellerby, L.M., Welsh, K., Xie, Z., Deveraux, Q.L., Salvesen, G.S., Bredesen, D.E., Rosenthal, R.E., Fiskum, G., and Reed, J.C. (1999). Release of caspase–9 from mitochondria during neuronal apoptosis and cerebral ischemia. Proc. Natl. Acad. Sci. U. S. A. 96, 5752–5757.
11. Aygok, G.A., Marmarou, A., Fatouros, P., Kettenmann, B., and Bullock, R.M. (2008). Assessment of mitochondrial impairment and cerebral blood flow in severe brain injured patients. Acta Neurochir. Suppl. 102, 57–61.
12. Xiong, Y., Gu, Q., Peterson, P.L., Muizelaar, J.P., and Lee, C.P. (1997). Mitochondrial dysfunction and calcium perturbation induced by traumatic brain injury. J. Neurotrauma 14, 23–34.
13. Sullivan, P.G., Krishnamurthy, S., Patel, S.P., Pandya, J.D., and Rabchevsky, A.G. (2007). Temporal characterization of mitochondrial bioenergetics after spinal cord injury. J. Neurotrauma 24, 991–999.
14. Bains, M., and Hall, E.D. (2012). Antioxidant therapies in traumatic brain and spinal cord injury. Biochim. Biophys. Acta 1822, 675–684.
15. Smith, R.A., Adlam, V.J., Blaikie, F.H., Manas, A.R., Porteous, C.M., James, A.M., Ross, M.F., Logan, A., Cocheme, H.M., Trnka, J., Prime, T.A., Abakumova, I., Jones, B.A., Filipovska, A., and Murphy, M.P. (2008). Mitochondria–targeted antioxidants in the treatment of disease. Ann. N. Y. Acad. Sci. 1147, 105–111.
16. Jin, H., Kanthasamy, A., Ghosh, A., Anantharam, V., Kalyanaraman, B., and Kanthasamy, A.G. (2014). Mitochondria–targeted antioxidants for treatment of Parkinson's disease: preclinical and clinical outcomes. Biochim. Biophys. Acta 1842, 1282–1294.
17. Patel, S.P., Sullivan, P.G., Pandya, J.D., Goldstein, G.A., VanRooyen, J.L., Yonutas, H.M., Eldahan, K.C., Morehouse, J., Magnuson, D.S., and Rabchevsky, A.G. (2014). N–acetylcysteine amide preserves mitochondrial bioenergetics and improves functional recovery following spinal trauma. Exp. Neurol. 257, 95–105.
18. Hall, E.D., Vaishnav, R.A., and Mustafa, A.G. (2010). Antioxidant therapies for traumatic brain injury. Neurotherapeutics 7, 51–61.
19. Robb, E.L., Winkelmolen, L., Visanji, N., Brotchie, J., and Stuart, J.A. (2008). Dietary resveratrol administration increases MnSOD expression and activity in mouse brain. Biochem. Biophys. Res. Commun. 372, 254–259.
20. Ungvari, Z., Labinskyy, N., Mukhopadhyay, P., Pinto, J.T., Bagi, Z., Ballabh, P., Zhang, C., Pacher, P., and Csiszar, A. (2009). Resveratrol attenuates mitochondrial oxidative stress in coronary arterial endothelial cells. Am. J. Physiol. Heart Circ. Physiol. 297, H1876–1881.
21. Ahmed, L.A., Shehata, N.I., Abdelkader, N.F., and Khattab, M.M. (2014). Tempol, a superoxide dismutase mimetic agent, ameliorates cisplatin–induced nephrotoxicity through alleviation of mitochondrial dysfunction in mice. PLoS One 9, e108889.
22. Xiong, Y., and Hall, E.D. (2009). Pharmacological evidence for a role of peroxynitrite in the pathophysiology of spinal cord injury. Exp. Neurol. 216, 105–114.
23. Sheu, S.S., Nauduri, D., and Anders, M.W. (2006). Targeting antioxidants to mitochondria: a new therapeutic direction. Biochim. Biophys. Acta 1762, 256–265.
24. Pandya, J.D., Readnower, R.D., Patel, S.P., Yonutas, H.M., Pauly, J.R., Goldstein, G.A., Rabchevsky, A.G., and Sullivan, P.G. (2014). N–acetylcysteine amide confers neuroprotection, improves bioenergetics and behavioral outcome following TBI. Exp. Neurol. 257, 106–113.
25. Jin, Y., McEwen, M.L., Nottingham, S.A., Maragos, W.F., Dragicevic, N.B., Sullivan, P.G., and Springer, J.E. (2004). The mitochondrial uncoupling agent 2,4–dinitrophenol improves mitochondrial function, attenuates oxidative damage, and increases white matter sparing in the contused spinal cord. J. Neurotrauma 21, 1396–1404.
26. Patel, S.P., Sullivan, P.G., Pandya, J.D., and Rabchevsky, A.G. (2009). Differential effects of the mitochondrial uncoupling agent, 2,4–dinitrophenol, or the nitroxide antioxidant, Tempol, on synaptic or nonsynaptic mitochondria after spinal cord injury. J. Neurosci. Res. 87, 130–140.
27. Rodriguez–Jimnez, F.J., Alastrue–Agudo, A., Erceg, S., Stojkovic, M., and Moreno–Manzano, V. (2012). FM19G11 favors spinal cord injury regeneration and stem cell self–renewal by mitochondrial uncoupling and glucose metabolism induction. Stem Cells 30, 2221–2233.
28. Sullivan, P.G., Springer, J.E., Hall, E.D., and Scheff, S.W. (2004). Mitochondrial uncoupling as a therapeutic target following neuronal injury. J. Bioenerg. Biomembr. 36, 353–356.
29. Maragos, W.F., Rockich, K.T., Dean, J.J., and Young, K.L. (2003). Pre– or post–treatment with the mitochondrial uncoupler 2,4–dinitrophenol attenuates striatal quinolinate lesions. Brain Res. 966, 312–316.
30. Brand, M.D., and Esteves, T.C. (2005). Physiological functions of the mitochondrial uncoupling proteins UCP2 and UCP3. Cell Metab. 2, 85–93.
31. Laird, M.D., Clerc, P., Polster, B.M., and Fiskum, G. (2013). Augmentation of normal and glutamate–impaired neuronal respiratory capacity by exogenous alternative biofuels. Transl. Stroke Res. 4, 643–651.
32. Carta, A., and Calvani, M. (1991). Acetyl–L–carnitine: a drug able to slow the progress of Alzheimer's disease? Ann. N. Y. Acad. Sci. 640, 228–232.
33. Puca, F.M., Genco, S., Specchio, L.M., Brancasi, B., D'Ursi, R., Prudenzano, A., Miccoli, A., Scarcia, R., Martino, R., and Savarese, M. (1990). Clinical pharmacodynamics of acetyl–L–carnitine in patients with Parkinson's disease. Int. J. Clin. Pharmacol. Res. 10, 139–143.
34. Liu, J., Head, E., Gharib, A.M., Yuan, W., Ingersoll, R.T., Hagen, T.M., Cotman, C.W., and Ames, B.N. (2002). Memory loss in old rats is associated with brain mitochondrial decay and RNA/DNA oxidation: partial reversal by feeding acetyl–L–carnitine and/or R–alpha –lipoic acid. Proc. Natl. Acad. Sci. U. S. A. 99, 2356–2361.
35. Petruzzella, V., Baggetto, L.G., Penin, F., Cafagna, F., Ruggiero, F.M., Cantatore, P., and Gadaleta, M.N. (1992). In vivo effect of acetyl–L–carnitine on succinate oxidation, adenine nucleotide pool and lipid composition of synaptic and non–synaptic mitochondria from cerebral hemispheres of senescent rats. Arch. Gerontol. Geriatr. 14, 131–144.
36. Patel, S.P., Sullivan, P.G., Lyttle, T.S., and Rabchevsky, A.G. (2010). Acetyl–L–carnitine ameliorates mitochondrial dysfunction following contusion spinal cord injury. J. Neurochem. 114, 291–301.
37. Patel, S.P., Sullivan, P.G., Lyttle, T.S., Magnuson, D.S., and Rabchevsky, A.G. (2012). Acetyl–L–carnitine treatment following spinal cord injury improves mitochondrial function correlated with remarkable tissue sparing and functional recovery. Neuroscience 210, 296–307.
38. McCully, J.D., Cowan, D.B., Emani, S.M., and Del Nido, P.J. (2017). Mitochondrial transplantation: From animal models to clinical use in humans. Mitochondrion 34, 127–134.
39. Gollihue, J.L. and Rabchevsky, A.G. (2017). Prospects for therapeutic mitochondrial transplantation. Mitochondrion 35, 70–79.
40. Masuzawa, A., Black, K.M., Pacak, C.A., Ericsson, M., Barnett, R.J., Drumm, C., Seth, P., Bloch, D.B., Levitsky, S., Cowan, D.B., and McCully, J.D. (2013). Transplantation of autologously derived mitochondria protects the heart from ischemia–reperfusion injury. Am. J. Physiol. Heart Circ. Physiol. 304, H966–982.
41. Pacak, C.A., Preble, J.M., Kondo, H., Seibel, P., Levitsky, S., Del Nido, P.J., Cowan, D.B., and McCully, J.D. (2015). Actin–dependent mitochondrial internalization in cardiomyocytes: evidence for rescue of mitochondrial function. Biol. Open 4, 622–626.
42. Cowan, D.B., Yao, R., Akurathi, V., Snay, E.R., Thedsanamoorthy, J.K., Zurakowski, D., Ericsson, M., Friehs, I., Wu, Y., Levitsky, S., Del Nido, P.J., Packard, A.B., and McCully, J.D. (2016). Intracoronary Delivery of Mitochondria to the Ischemic Heart for Cardioprotection. PLoS One 11, e0160889.
43. Hayakawa, K., Esposito, E., Wang, X., Terasaki, Y., Liu, Y., Xing, C., Ji, X., and Lo, E.H. (2016). Transfer of mitochondria from astrocytes to neurons after stroke. Nature 535, 551–555.

44. Shi, X., Zhao, M., Fu, C., and Fu, A. (2017). Intravenous administration of mitochondria for treating experimental Parkinson's disease. Mitochondrion 34, 91–100.
45. Chang, J.C., Wu, S.L., Liu, K.H., Chen, Y.H., Chuang, C.S., Cheng, F.C., Su, H.L., Wei, Y.H., Kuo, S.J. and Liu, C.S. (2016). Allogeneic/xenogeneic transplantation of peptide–labeled mitochondria in Parkinson's disease: restoration of mitochondria functions and attenuation of 6–hydroxydopamine–induced neurotoxicity. Transl. Res. 170, 40–56 e41–43.
46. Gollihue, J.L., Patel, S.P., Mashburn, C., Eldahan, K.C., Sullivan, P.G. and Rabchevsky, A.G. (2017). Optimization of mitochondrial isolation techniques for intraspinal transplantation procedures. J. Neurosci. Methods 287, 1–12.
47. Scheff, S.W., Rabchevsky, A.G., Fugaccia, I., Main, J.A., and Lumpp, J.E., Jr. (2003). Experimental modeling of spinal cord injury: characterization of a force–defined injury device. J. Neurotrauma 20, 179–193.
48. Basso, D.M., Beattie, M.S., and Bresnahan, J.C. (1995). A sensitive and reliable locomotor rating scale for open field testing in rats. J. Neurotrauma 12, 1–21.
49. Chaplan, S.R., Bach, F.W., Pogrel, J.W., Chung, J.M., and Yaksh, T.L. (1994). Quantitative assessment of tactile allodynia in the rat paw. J. Neurosci. Methods 53, 55–63.
50. Intondi, A.B., Dahlgren, M.N., Eilers, M.A., and Taylor, B.K. (2008). Intrathecal neuropeptide Y reduces behavioral and molecular markers of inflammatory or neuropathic pain. Pain 137, 352–365.
51. Brightwell, J.J., and Taylor, B.K. (2009). Noradrenergic neurons in the locus coeruleus contribute to neuropathic pain. Neuroscience 160, 174–185.
52. Sauerbeck, A., Pandya, J., Singh, I., Bittman, K., Readnower, R., Bing, G., and Sullivan, P. (2011). Analysis of regional brain mitochondrial bioenergetics and susceptibility to mitochondrial inhibition utilizing a microplate based system. J. Neurosci. Methods 198, 36–43.
53. Rabchevsky, A.G., Fugaccia, I., Sullivan, P.G., and Scheff, S.W. (2001). Cyclosporin A treatment following spinal cord injury to the rat: behavioral effects and stereological assessment of tissue sparing. J. Neurotrauma 18, 513–522.
54. Rabchevsky, A.G., Fugaccia, I., Sullivan, P.G., Blades, D.A., and Scheff, S.W. (2002). Efficacy of methylprednisolone therapy for the injured rat spinal cord. J. Neurosci. Res. 68, 7–18.
55. Michel, R.P., and Cruz–Orive, L.M. (1988). Application of the Cavalieri principle and vertical sections method to lung: estimation of volume and pleural surface area. J. Microsc. 150, 117–136.
56. Hou, S., Duale, H., Cameron, A.A., Abshire, S.M., Lyttle, T.S., and Rabchevsky, A.G. (2008). Plasticity of lumbosacral propriospinal neurons is associated with the development of autonomic dysreflexia after thoracic spinal cord transection. J. Comp. Neurol. 509, 382–399.
57. Chang, J., Liu, K., Chuang, C., Wu, S., Kuo, S., and Liu, C. (2013). Transplantation of Pep–1–labeled mitochondria protection against a 6–OHDA–induced neurotoxicity in rats. Changhua J. Med. 11, 8–17.
58. McCullers, D.L., Sullivan, P.G., Scheff, S.W., and Herman, J.P. (2002). Mifepristone protects CA1 hippocampal neurons following traumatic brain injury in rat. Neuroscience 109, 219–230.
59. Kaza, A.K., Wamala, I., Friehs, I., Kuebler, J.D., Rathod, R.H., Berra, I., Ericsson, M., Yao, R., Thedsanamoorthy, J.K., Zurakowski, D., Levitsky, S., Del Nido, P.J., Cowan, D.B., and McCully, J.D. (2016). Myocardial rescue with autologous mitochondrial transplantation in a porcine model of ischemia/reperfusion. J. Thorac. Cardiovasc. Surg. 153, 934–943.
60. Muramatsu, R., and Yamashita, T. (2014). Pericyte function in the physiological central nervous system. Neurosci. Res. 81–82, 38–41.
61. Winkler, E.A., Bell, R.D., and Zlokovic, B.V. (2011). Central nervous system pericytes in health and disease. Nat. Neurosci. 14, 1398–1405.
62. Armulik, A., Genove, G., and Betsholtz, C. (2011). Pericytes: developmental, physiological, and pathological perspectives, problems, and promises. Dev. Cell 21, 193–215.
63. Hamilton, N.B., Attwell, D., and Hall, C.N. (2010). Pericyte–mediated regulation of capillary diameter: a component of neurovascular coupling in health and disease. Front. Neuroenergetics 2, pii 5.
64. Fernandez–Vizarra, E., Enriquez, J.A., Perez–Martos, A., Montoya, J., and Fernandez–Silva, P. (2011). Tissue–specific differences in mitochondrial activity and biogenesis. Mitochondrion 11, 207–213.
65. Magnuson, D.S., Lovett, R., Coffee, C., Gray, R., Han, Y., Zhang, Y.P., and Burke, D.A. (2005). Functional consequences of lumbar spinal cord contusion injuries in the adult rat. J. Neurotrauma 22, 529–543.
66. Garg, A.D., Nowis, D., Golab, J., Vandenabeele, P., Krysko, D.V., and Agostinis, P. (2010). Immunogenic cell death, DAMPs and anticancer therapeutics: an emerging amalgamation. Biochim. Biophys. Acta 1805, 53–71.
67. Schwartz, M. (2003). Macrophages and microglia in central nervous system injury: are they helpful or harmful? J. Cereb. Blood Flow Metab. 23, 385–394.
68. Markiewicz, I., and Lukomska, B. (2006). The role of astrocytes in the physiology and pathology of the central nervous system. Acta Neurobiol. Exp. 66, 343–358.
69. Baumann, N., and Pham–Dinh, D. (2001). Biology of oligodendrocyte and myelin in the mammalian central nervous system. Physiol. Rev. 81, 871–927.
70. Tata, M., Ruhrberg, C., and Fantin, A. (2015). Vascularisation of the central nervous system. Mech. Dev. 138, Pt. 1, 26–36.
71. Gollihue, J.L., and Rabchevsky, A.G. (2017). Prospects for therapeutic mitochondrial transplantation. Mitochondrion 35, 70–79.
72. Clark, M.A., and Shay, J.W. (1982). Mitochondrial transformation of mammalian cells. Nature 295, 605–607.
73. Katrangi, E., D'Souza, G., Boddapati, S.V., Kulawiec, M., Singh, K.K., Bigger, B., and Weissig, V. (2007). Xenogenic transfer of isolated murine mitochondria into human rho0 cells can improve respiratory function. Rejuvenation Res. 10, 561–570.
74. Chang, J.C., Liu, K.H., Li, Y.C., Kou, S.J., Wei, Y.H., Chuang, C.S., Hsieh, M., and Liu, C.S. (2013). Functional recovery of human cells harbouring the mitochondrial DNA mutation MERRF A8344G via peptide–mediated mitochondrial delivery. Neurosignals 21, 160–173.
75. Islam, M.N., Das, S.R., Emin, M.T., Wei, M., Sun, L., Westphalen, K., Rowlands, D.J., Quadri, S.K., Bhattacharya, S., and Bhattacharya, J. (2012). Mitochondrial transfer from bone–marrow–derived stromal cells to pulmonary alveoli protects against acute lung injury. Nat. Med. 18, 759–765.
76. Koyanagi, M., Brandes, R.P., Haendeler, J., Zeiher, A.M., and Dimmeler, S. (2005). Cell–to–cell connection of endothelial progenitor cells with cardiac myocytes by nanotubes: a novel mechanism for cell fate changes? Circ. Res. 96, 1039–1041.
77. Wang, X. and Gerdes, H.H. (2015). Transfer of mitochondria via tunneling nanotubes rescues apoptotic PC12 cells. Cell Death Differ. 22, 1181–1191.

Address correspondence to:
Alexander G. Rabchevsky, PhD
Spinal Cord and Brain Injury Research Center
University of Kentucky
B471, BBSRB
741 S. Limestone
Lexington, KY 40536–0509

E-mail: agrab@uky.edu